12-2008

Air Demand in Free Flowing Gated Conduits

David Peter Oveson
Utah State University

AIR DEMAND IN FREE FLOWING GATED CONDUITS

by

D. Peter Oveson

A thesis submitted in partial fulfillment
of the requirements for the degree

of

MASTER OF SCIENCE

in

Civil and Environmental Engineering

Approved:

Steven L. Barfuss Major Professor	Blake P. Tullis Committee Member
Mac Mckee Committee Member	Byron R. Burnham Dean of Graduate Studies

UTAH STATE UNIVERSITY
Logan, Utah

2008

ABSTRACT

Air Demand in Free Flowing Gated Conduits

by

D. Peter Oveson, Master of Science

Utah State University, 2008

Major Professor: Steven L. Barfuss
Department: Civil and Environmental Engineering

A physical experimental setup of a circular, gated closed conduit was built at the Utah Water Research Laboratory (UWRL). Setup configurations were modified and data were measured to aid in the study of physical variables on air demand. It was determined that gate opening, gate and water surface roughness, and conduit length all were significant variables on the air demand measured through the conduit air vent. It was also determined that no noticeable air velocity profile existed above the air-water interface. A linear relationship was found between the air flow rate to water flow rate ratio (air-demand ratio) and head-to-gate height ratio when identical conduit geometry was used. Data obtained from this study illustrated that the use of the Froude number is an incomplete way to quantify air demand due to the effects of changing conduit geometry.

(82 pages)

ACKNOWLEDGMENTS

I would like to thank my wife, Sandy, for all of her support in my desire to get a graduate degree. I would like to thank Steve Barfuss for employing me at the UWRL and giving me the initial idea for this research as well as providing invaluable direction along the way. I would also like to thank my committee members, Blake Tullis and Mac McKee, for their support and assistance in helping to make this a quality research project. Hank Falvey has also been an important advisor and I give my sincere thanks to him for his advice and direction. I addition to those listed I would like to thank all of my family, friends, professors, co-workers, and fellow students that have provided support throughout this project.

D. Peter Oveson

CONTENTS

Page

LIST OF TABLES

LIST OF FIGURES

LIST OF ACRONYMS AND ABBREVIATIONS

cfs	cubic feet per second
cms	cubic meters per second
fps	feet per second
ft	feet
kg	kilo grams
lb	pound force
m	meter
mA	mili-amps
mps	meters per second
N	newton
PVC	Polyvinyl Chloride
s	seconds
USACE	United States Army Corps of Engineers
UWRL	Utah Water Research Laboratory

LIST OF SYMBOLS

α	Angle conduit makes with the horizontal
A	Cross-sectional area of pipe, ft (m)
C_d	Orifice discharge coefficient
δ	Boundary layer thickness ft, (m)
Δh	Head loss differential across orifice plate, ft (m)
d	Diameter of orifice throat, ft (m)
D	Diameter of pipe, ft (m)
Fr	Froude number
γ	Specific weight of water lb/ft^3, (N/m^3)
g	Acceleration due to gravity, ft/s^2 (m/s^2)
H	Total energy head, ft (m)
h_g	Gate opening height, ft (m)
v	Maximum water surface velocity conduit, fps (mps)
n_v	Coefficient relating to water surface roughness
P	Static pressure in pipe, lb/ft^2 (N/m^2)
Q_a	Air flow rate measured through air vent, cfs (cms)
Q_w	Water flow rate in conduit, cfs (cms)
ρ_w	Density of water, slugs/ft^3 (kg/m^3)
Re	Reynolds number of discharge or flow rate
R_w	Average water surface roughness in conduit, in (cm)

σ	Interfacial surface tension, lb/ft (N/m)
Tw	Top width of water prism ft, (m)
u	Local air velocity, fps (mps)
V	Mean velocity, fps (mps)
W	Weber number
x	Length of conduit downstream of gate, ft (m)
y_a	Distance from the water surface ft, (m)
Y	Flow depth, ft (m)

CHAPTER 1

INTRODUCTION

This study was performed in an effort to better understand the driving mechanisms of air demand in gated closed conduits with free surface open channel flow conditions. Research for this study was conducted in conjunction with a U.S. Army Corps of Engineers physical model of the Lake Success Dam outlet works. Many researchers have studied air demand in closed conduits and outlet works. Despite this fact, knowledge of the topic remains limited; the subject of air demand in outlet works remains a difficult and misunderstood topic for many design engineers. This is likely due to the general lack of information regarding the driving mechanisms of air demand in such a system.

The research in this report has primarily been focused on the relationship between air demand in a gated closed conduit and several variables including: gate opening, conduit length, conduit slope, and water surface roughness. It is the goal of the author that a greater understanding of the driving forces and knowledge of the effects of variables on air demand in closed conduits will aid future designers when estimating the maximum air demand for a specific design.

Background

The primary application for this research deals with the design of low-level outlet works or bottom outlets for dams although application can be extended to any similar design. Low-level outlet works typically extend from a low elevation in the reservoir

pool to the downstream side of the dam. This hydraulic structure is the means for many reservoirs to provide water supply, flood control, low-level flow requirements, irrigation requirements, power generation, and drawdown of reservoir pool for maintenance and repair (USACE, 1980).

Typical elements of a reservoir outlet works for an earth dam consist of an intake structure, pressurized reach of conduit, control gate, air vent, and non-pressurized reach of conduit (see Figure 1). An air vent is typically placed downstream of the control gate to prevent cavitation damage to the gate and gate structure (USACE, 1980). Total air demand refers to the amount of air that the flowing water pulls into the conduit through the air vent and downstream exit portal (Speerli, 1999). It is important to appropriately quantify the air demand to prevent negative impacts. If an air vent is sized too small, it can cause a greater amount of head loss and greater occurrence of negative pressure immediately downstream of the gate; negative pressures increase the possibility for cavitation damage (Falvey, 1980). Knowing the range of air demand will aid in sizing the air vent appropriately.

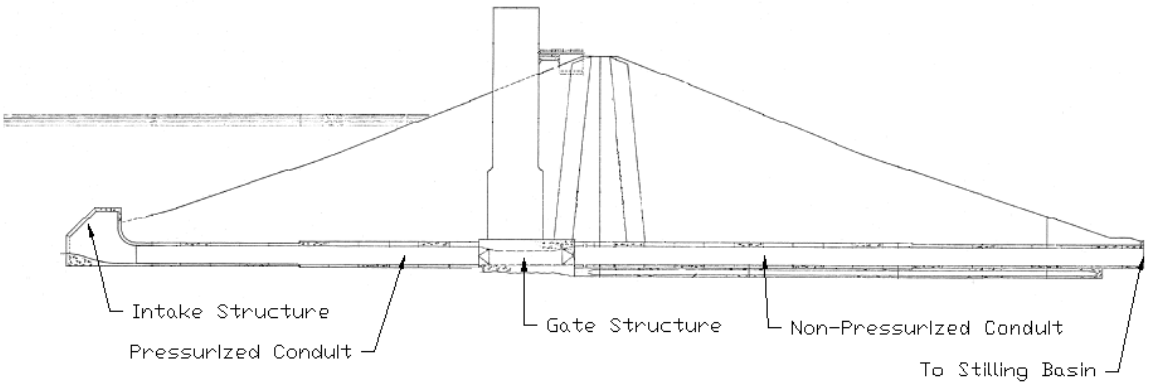

Figure 1. Low-level outlet works overview.

Many researchers have studied this problem and developed empirical equations that can be used to estimate air demand. Although some basic understanding of the problem has been obtained from these studies and the equations derived, there remains a large amount of uncertainty in prototype and model data observed. Specifically, no attempts have been made to classify data in terms of the geometric characteristics of each design. For example, the outlet works data for both circular and rectangular conduit cross-sections have often been combined to create empirical equations. In addition to the uncertainty of the developed empirical equations, several conflicting theories suggest the cause of air demand, but none seem to be accurate enough to dispel the others.

Objective

The purpose of this research was to determine the effects of specific physical variables on air demand for a physical experiment of a gated closed conduit. This objective was achieved by building a physical experimental setup, conducting experiments, obtaining data, analyzing the data, and presenting the results. The experimental results were compared to several approaches in the available literature. Designers can use the results of this study to improve on the methods of practice or as a base for future research.

Research Scope

This research was limited to studying the relationship between air demand and several physical model variables on a single installation. This research does not attempt

to study or develop a general relationship for air demand in all gated closed conduits, but rather to give insight and understanding into some of the factors that affect the relationship. This research dealt specifically with gated closed *circular* conduits, which are commonly used for many dam outlet works. Results taken from this study may not apply directly to channel or gate cross-sectional geometries that were not considered. The design and sizing of the air intake vent was not discussed in this report; only variables that cause changes in the amount of air drawn in through the air vent were studied. The physical experimental setup, methods, and procedures used in this study are described in detail in Chapter 4.

Overview

In order to ensure that this study is consistent with work previously done on the subject, an in-depth literature review was conducted. Chapter 2 is comprised of the literature review and outlines the significant and related findings from previous studies. The basic theory and reasoning behind the methods used in presenting results is also included in the literature review. Chapter 3 consists of an in-depth discussion of the physical experimental setup used to conduct research for this study. Other aspects relating to the experimental setup are also included in Chapter 3, such as data measurement and collection. Experimental results are discussed and shown in Chapter 4. The data obtained from this experiment is validated in comparison to several studies in Chapter 5. Chapter 6 presents a brief summary, conclusions, and recommendations for further research.

CHAPTER 2

LITERATURE REVIEW AND THEORY

Literature Review

One of the first known studies of air demand in closed conduits was conducted by Kalinske and Robertson (1943). It suggested a hydraulic jump as a means to remove air pockets from pipelines, and quantified how much air a hydraulic jump that filled the entire conduit could remove through air entrainment. The research determined that air entrainment was a function of the Froude number upstream of the hydraulic jump.

Kalinske and Robertson determined an empirical relationship that described the air demand to water discharge ratio (air-demand ratio) verses Froude number for their physical model; the following empirical equation was suggested:

$$\frac{Q_a}{Q_w} = 0.0066 \cdot (Fr - 1)^{1.4} \tag{1}$$

where:

Q_a Air flow rate measured through air vent, cfs (cms)

Q_w Water flow rate in conduit, cfs (cms)

Fr Froude number

where:

$$Fr = \frac{V}{\sqrt{g \cdot Y}} \tag{2}$$

V Mean water velocity, fps (mps)

g Acceleration due to gravity, ft/s^2 (m/s^2)

Y Water depth, ft (m)

In hydraulic jump flow that filled the conduit, the air demand ratio was independent of the gate opening and conduit slope. Other researchers have since verified the work of Kalinske and Robertson (Sharma, 1976). If applied to free surface flow, Equation (1) has been shown to act as a minimum envelope curve for the air demand ratio. This phenomenon was pointed out by Ghetti and Di Silvio (1967) which found that free surface air demand never dropped below the air demand of fully pressurized hydraulic jump flow.

The U.S. Army Corps of Engineers (1964) developed a relationship for free surface air demand and the Froude number based on prototype data from several dams. The following empirical equation was determined:

$$\frac{Q_a}{Q_w} = 0.3 \cdot (Fr - 1)^{1.06} \tag{3}$$

Many additional researchers have verified prototype data with laboratory tests for free surface flow and determined empirical equations similar to Equation (3). Sharma (1976) verified prototype data with a laboratory experiment and compared results with the empirical equations found in other studies. A linear envelope curve based on the Froude number at the vena contracta described the upper limit for the air-demand ratio for all data and empirical equations:

$$\frac{Q_a}{Q_w} = 0.09 \cdot Fr \tag{4}$$

Campbell and Guyton (1953) suggested that the free water surface produced a drag force on the air mass above the water surface. Due to the drag force on the air mass,

it was concluded that the air velocity had a logarithmic profile above the water surface that ranged from the water velocity at the water surface to zero at the pipe wall boundary. Sharma (1976) found that the assumption of a logarithmic velocity profile defined by Campbell and Guyton was not accurate due to the fact that it always underestimated prototype data. Sharma also studied the air velocity profile above the water surface using high-speed film photography of water droplets and assuming that the velocity of the water droplets was equal to the velocity of the air, but did not determine any velocity profile.

Many researchers since Campbell and Guyton have tried to expand on the theory of a defined air profile above the water surface. Sikora (1965) as cited in Falvey (1980) assumed that the air above the water surface in the conduit would not exceed the mean water velocity. The air mass above the water is assumed to travel at the mean velocity of the water surface. The flow rate of air above the water surface is found through multiplying the mean water surface velocity by the minimum air cross-sectional area in the conduit. This method has been found to overestimate air demand when compared to prototype data, but is often used as an upper bound for air demand (Mifkovic, 2007).

Falvey (1980) built on the work of Campbell and Guyton by suggesting that the height of the upper boundary layer of zero air velocity varied with distance from the gate and was not simply the conduit boundary as previously described. The following equations describe the velocity profile and the development of the boundary layer:

$$\frac{u}{v_{\max}} = 1 - \left(\frac{y_a}{\delta} \right)^{1/n_v} \tag{5}$$

where:

u Local air velocity, fps (mps)

v_{max} Maximum water surface velocity in the conduit, fps (mps)

y_a Distance from the water surface ft, (m)

n_v Coefficient between 5.4 and 10 relating to water surface roughness

δ Boundary layer thickness ft, (m)

where:

$$\delta = 0.01 \cdot x \tag{6}$$

x Length of conduit downstream of gate, ft (m)

In the analysis of Warm Springs Dam and other prototype data, this method has been found to underestimate prototype air demand, but can be used as a lower bound for air demand (Mifkovic, 2007).

Ghetti and Di Silvio (1967) studied air demand in several Italian dams. They found that air entrainment into the water was a significant driving factor of air demand. In order to estimate the air entrainment in free surface flow in a closed conduit, Falvey (1980) suggests using the following equation determined for spillways:

$$\frac{Q_a / Q_w}{Q_a / Q_w - 1} = 0.05 \cdot Fr - \frac{\sqrt{\sin \alpha} \cdot W}{63 \cdot Fr} \tag{7}$$

where:

α Angle conduit makes with the horizontal

W Weber number

where:

$$W = \frac{V}{\left(\sigma / \rho_W \cdot Y\right)} \tag{8}$$

σ Interfacial surface tension, lb/ft (N/m)

ρ_W Density of water, slugs/ft^3 (kg/m^3)

Speerli (1999) also found that air demand is largely a function of air entrainment into the water. This study shows that the total air demand is the sum of air entering through the air vent and exit portal of the conduit. It was determined that the total air demand is independent of air vent size, and that when air vent losses increase additional air will be supplied through the exit portal. Speerli and Hager (2000) studied air concentration due to entrainment in relation to total distance from the gate. It was found that the maximum amount of air concentration in the water occurred during the first portion of conduit immediately downstream of the gate, after which point a small portion of air detrainment occurred.

In addition to the dependence of the air demand ratio on the Froude number, several researchers have suggested the importance of other parameters in the air demand. Wunderlich (1961) as cited in Sharma (1976) suggested that the ratio of the cross-sectional water area at the vena contracta to cross-sectional conduit area also influenced the air-demand ratio. The following equation describes the relationship between the air demand ratio and flow area at the vena contracta for free surface flow:

$$1 - \frac{Q_a}{Q_w} = \frac{1}{A_c / A_t} \tag{9}$$

where:

A_c Cross-sectional area of water prism at the vena contracta, ft^2 (m^2)

A_t Cross-sectional area of the conduit, ft^2 (m^2)

Lysne and Guttormsen (1971) also studied the relationship between the cross-sectional areas of water to the cross-sectional area of the conduit and developed the following envelope curve based on prototype data:

$$1+\frac{Q_a}{Q_w}=1.2\cdot\left(\frac{1}{A_c/A_t}\right)^{0.2} \tag{10}$$

Winser (1965) as cited in Sharma (1976) suggested that the air demand ratio was also dependent on the ratio of the cross-sectional area of the air vent to the cross-sectional area of the conduit. Winser concluded that when the air vent to conduit area ratio was greater than 1/40 that air demand was only a function of the Froude number (see Equation (11)). Although, when the same ratio was less than 1/5000 the air demand was found to be only a function of the air vent to conduit area. The following equation was given by Winser to describe air demand for free surface flow in relation to the Froude number for air vent to conduit area ratios greater than 1/40:

$$\frac{Q_a}{Q_w}=0.24\cdot(Fr-1)^{1.4} \tag{11}$$

Speerli and Hager (2000), Falvey (1980), and Sharma (1976) all outline additional literature that was deemed unrelated or unnecessary to the current study on free surface

air demand; these papers contain a wealth of additional information regarding spray and hydraulic jump flow, both of which are not discussed in this paper. It is evident from the literature that there is limited knowledge relating to the study of the effects of conduit slope, conduit length, and water surface roughness to the air demand ratio. There is also much debate among researchers as to the nature, if any, of the air velocity profile above the free water surface.

Theory Applied in This Study

The air flow rate to water flow rate ratio (Q_a/Q_w) is referred to as the air-demand ratio and will be used to illustrate air demand measured in the model at the air intake pipe. The ratio of the total head at the upstream side of the gate over the height of the gate opening is referred to as the head-to-gate ratio (H/h_g) and can be used to describe the hydraulic characteristics of the flow upstream of the gate. As illustrated by Finnemore and Franzini (2002), the total head is obtained by using the following equation:

$$H = \frac{P}{\gamma} + \frac{V^2}{2 \cdot g} \tag{12}$$

where:

H	Total head immediately upstream of control gate, ft (m)
P	Static Pressure in the pipe upstream of control gate, lb/ft^2 (N/m^2)
γ	Specific weight of water lb/ft^3, (N/m^3)
V	Mean flow velocity upstream of control gate, fps (mps)
g	Acceleration due to gravity ft/s^2 (m/s^2)

The head-to-gate ratio was chosen to represent the hydraulic characteristics upstream of the gate because it is a dimensionless parameter that influences the water discharge rate through the system. Most previous studies on air demand in closed conduits have included some representation of a reservoir and have related reservoir pool elevation or total energy head to air demand (Speerli, 1999). Because no reservoir was modeled in this study, total energy head, immediately upstream of the gate, was used according to Equation (12).

The head-to-gate ratio also represents a theoretical squared Froude number downstream of the gate (Ghetti and Di Silvio, 1967). Using the head-to-gate ratio limits the analysis to the specific conduit geometry tested, because it represents a unit width that doesn't take changing channel geometry into account (i.e. it would be difficult to relate a circular channel to a rectangular channel using the head to gate ratio). The uncertainty and error of data obtained upstream of the gate (i.e. flow rate, piezometric pressure, conduit diameter, and gate opening) is smaller than that of data obtained downstream of the gate (i.e. free surface flow depth). This is due to visual limitations in obtaining water surface depth measurements and will be discussed later in this report. Due to the greater accuracy of measurements upstream of the gate the head-to-gate ratio will be used to relate the air-demand ratio between runs with identical test configurations.

The Froude number (Fr), found through Equation (2), and is the preferred way to relate to the air demand ratio in the literature. The Froude number is a dimensionless number which considers inertia and gravity forces and does not consider viscous or surface tension forces. The importance of the Froude number on air demand might be

illustrated by the model parameters that are used in its computation, which include: velocity, length, and gravity (Finnemore and Franzini, 2002). Although the best indication of the relevance of the Froude number to air demand comes from plotting the air-demand ratio in relation to the Froude number. As will be seen in this study significant correlation exists between the two data sets. When air demand data from this experimental setup is plotted against the Reynolds number or Weber number there is no evidence that any relationship exists. The lack of any relationship between Reynolds and Weber numbers and the air-demand ratio has also been found by previous studies (Ghetti and Di Silvio, 1967).

In order to give the best and most accurate presentation of the results of this study, air demand will be plotted against the head to gate ratio for runs with similar channel geometry and against the Froude number for runs with different conduit geometry. This will not only enable the researcher to utilize the most accurate air demand relationships, but will also ensure that air demand comparisons between different conduit geometry remain valid. The Froude number will be calculated by using Equation (2) using the effective depth in the conduit. The effective depth is defined by Falvey (1980) as follows:

$$Y_e = \frac{A}{T_w} \tag{13}$$

where:

Y_e Effective depth, ft (m)

A Mean cross-sectional area of water prism, ft^2 (m^2)

T_w Mean top-width of water prism, ft (m)

In the literature the Froude number has often been based on the vena contracta in relation to the air-demand ratio (Sharma, 1976). The effective depth is used to calculate the Froude number for open channel air entrainment (Falvey, 1980). In this study, the Froude number was based on the effective depth in the conduit because the exact contraction coefficient was not known for each individual gate opening and it was assumed that a large amount of the air demand would be driven by air entrainment.

CHAPTER 3

PHYSICAL EXPERIMENTAL SETUP AND DATA COLLECTION

Physical Experimental Setup

All testing was performed in a physical experimental setup constructed at the Utah Water Research Laboratory (UWRL). A drawing which shows all model components is shown in Figure 2. The model consisted of a 12-in diameter PVC pipeline with adjustable length and slope. Water was supplied to the pipeline through the UWRL water supply system, which received water from First Dam Reservoir. Water entered the pipeline through two parallel 8-in diameter supply pipes that feed one common 12-in diameter pipe. Flow metering was provided by two orifice meters, one installed in the primary 8-in diameter supply line and one installed in the combined 12-in diameter supply line.

Downstream of the orifice meters a 12-in butterfly valve provided flow control for the model. A 12-in diameter flexible rubber expansion joint was installed downstream of the control valve, the joint enabled the pipeline slope to vary from horizontal to a 13.33 percent slope. Figure 3 shows a side view of the installed rubber expansion joint. Along the entire length of the conduit, adjustable stands were used to easily adjust and set the slope of the conduit. The slope was set and verified using standard survey equipment.

A gate which simulated an outlet works control gate was installed 3.75 diameters downstream of the flexible rubber expansion joint. Individual gates representing openings of 10, 30, 50, 70, and 90 percent of the cross-sectional conduit area were used

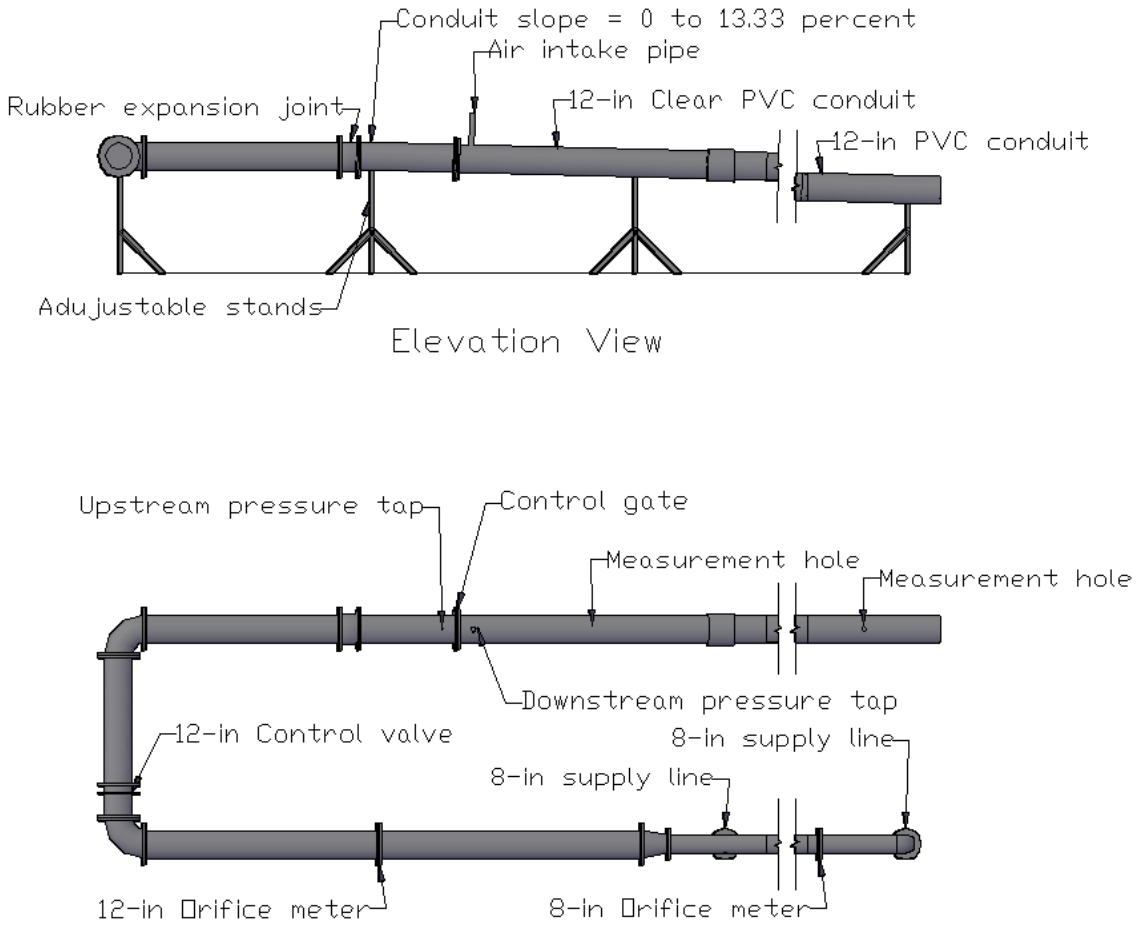

Figure 2. Physical model overview.

to simulate a range of gate openings (see Figure 4). The bottom of each gate was rectangular and had a width of 0.5 in. In addition to regular smooth gates, a 50 percent serrated gate opening was fabricated with 0.991-in serrated teeth in order to increase the water surface roughness. Each gate was machined out of clear acrylic in order to act similar to a control gate with no gate slots or interruption in the invert or side wall geometry (see Figure 4).

An air intake pipe was installed immediately downstream of the gate. The air intake pipe consisted of a 2.02-in inside diameter pipe that had a total length of 12-in.

Figure 3. Flexible rubber expansion joint.

The pipe was installed directly into the crown of the 12-in PVC pipe. A 0.375-in diameter hole was drilled into the side of the pipe at a location of 4-in from the crown to allow insertion of the air velocity probe used to measure the air flow rate though the air intake pipe. A gate valve was installed near the top of the air intake pipe and all data in this report was all taken with the gate valve at a full open position. Figure 5 shows the air intake piping setup.

Pressure taps were located upstream and downstream of the gate location. The tap upstream of the gate was used to determine the hydraulic grade line or piezometric pressure of the pipeline just before the gate. The tap downstream of the gate and air

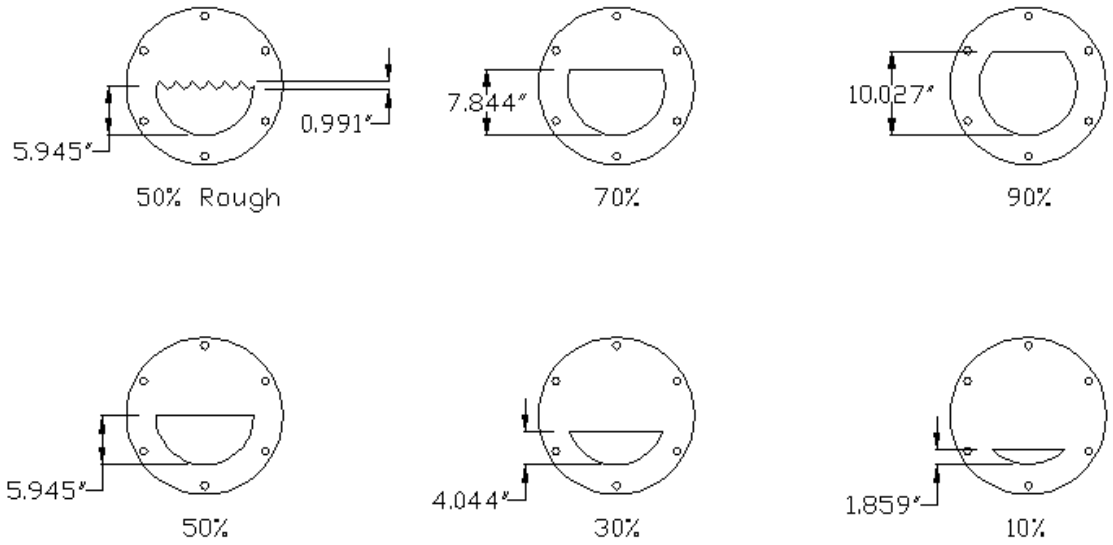

Figure 4. Gate dimension drawings.

Figure 5. Air intake setup (looking upstream).

intake was used to determine the pressure on the crown of the pipe above the free water surface. This can be seen in Figure 5.

The pipeline was constructed of three schedule 40 12-in diameter PVC sections connected end to end. The first PVC section was clear to provide flow visualization downstream of the gate and air intake and was approximately 10 ft in length (see Figure 6). The second and third pipe sections were non-transparent white PVC and were both 19 ft in length.

In order to provide access to the pipeline for depth, water surface roughness, and air velocity measurements, five 2.25-in diameter holes were drilled into the crown of the pipeline. The first hole was located 5 ft downstream of the control gate with each

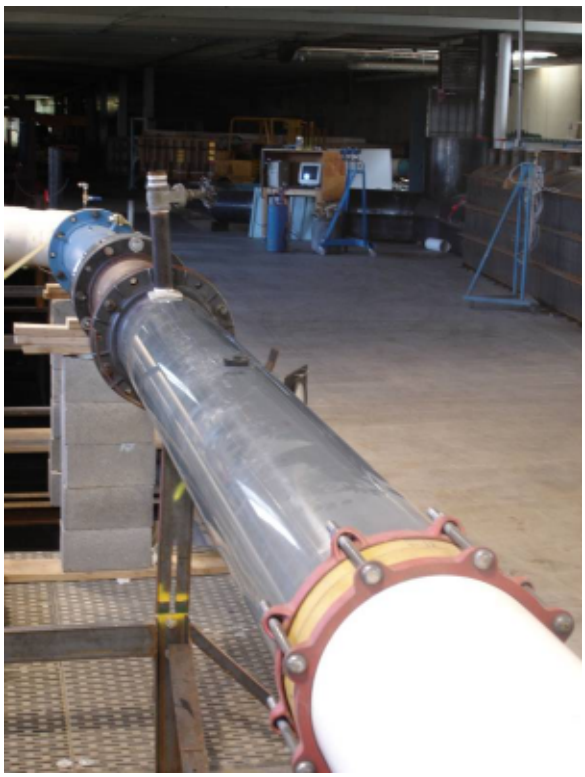

Figure 6. Clear PVC conduit section (looking upstream).

successive hole located at 10 ft intervals along the crown of the conduit. Rubber stoppers were used to seal the holes to ensure that air or water did not enter or exit the pipeline while taking air demand measurements. Figure 7 shows a 2.25-in diameter access hole and rubber stopper. A 0.375-in diameter hole was drilled into the center of each rubber stopper to allow air velocity probe access into the pipe for taking measurements of the air column velocities above the water surface without admitting additional air at the measurement location.

An end cap or cover was machined out of clear acrylic and was installed at the exit portal of the conduit. The cover could be adjusted from a full open position to a position at the depth of the water running out of the conduit blocking off the section of free air above the water surface. Figure 8 shows the acrylic end cover in a semi-closed position. This was used to determine the amount of air demand that was traveling above

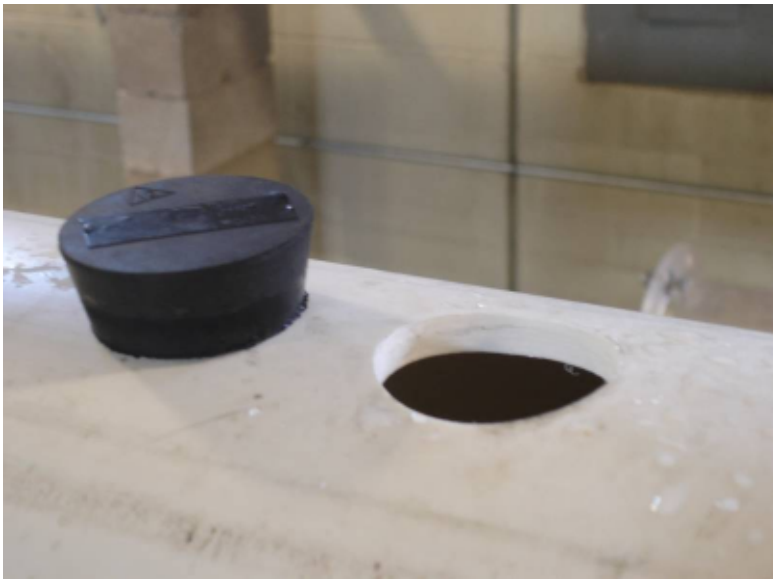

Figure 7. Measurement hole.

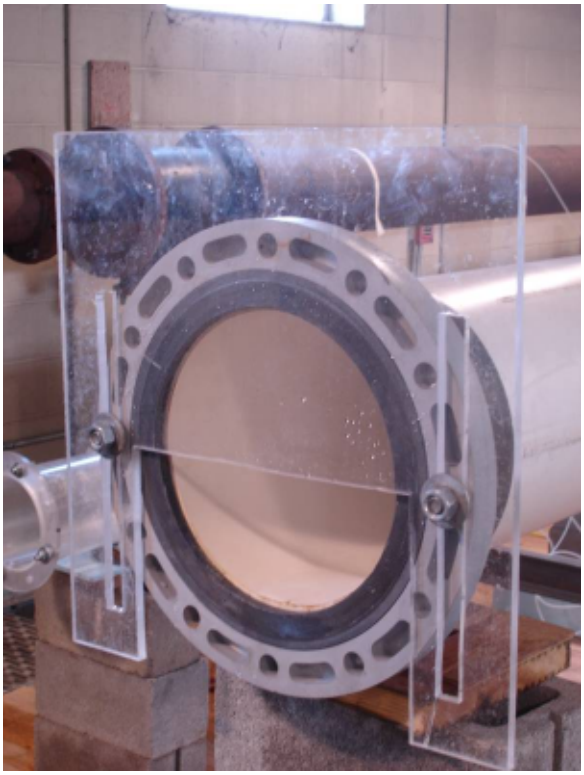

Figure 8. Acrylic end cap.

the water surface. Data was obtained with and without the end cap in place for most test runs.

Data Measurements

Several measurements were made in order to obtain sufficient data to perform this research. Experimental data collected included: water flow rate, upstream piezometric pressure, downstream air pressure, air flow rate, air velocity profile at each access hole, water surface and turbulence roughness depth, and end cap location. A brief discussion and outline of the procedure used to obtain each measurement will be provided.

Additionally, any concerns relating to the accuracy of each measurement will be discussed.

Water flow rate

Experimental water flow rate (Q_w) was an essential measurement which was used to calculate the air demand ratio (Q_a/Q_w). It was found by measuring the pressure differential across an orifice plate. Orifice calibration data is available in Appendix A. The differential pressure was measured between flange taps upstream and downstream of each orifice. Calibrated pressure transmitters were used to convert the pressure differential to a 4-to-20 mA signal, which was reported using a calibrated multi-meter.

In order to obtain a flow measurement for each test run, pressure transmitters were zeroed at a no flow condition and the 4-to-20 signal range was verified prior to every data collection session. All tubing used were bled to remove all air bubbles. The average 4-to-20 signal displayed on the multi-meter was recorded. The signal was then converted to the head loss across the orifice plate, which was used to determine the flow rate. The orifice equation used to determine the flow rate is as follows:

$$Q = C_d \cdot A_o \cdot \frac{\sqrt{2 \cdot g \cdot \Delta h}}{1 - \left(d/D\right)^4} \tag{14}$$

where:

Q Discharge or flow rate, cfs (cms)

C Orifice discharge coefficient

A_O Cross-sectional area of orifice throat, ft^2 (m^2)

g Acceleration due to gravity, ft/s^2 (m/s^2)

Δh Head loss differential across orifice plate, ft (m)

d Diameter of orifice throat, ft (m)

D Diameter of pipe, ft (m)

Upstream piezometric pressure

The piezometric pressure was measured to determine the static head upstream of the gate. This was found through a pressure tap located upstream of the gate that was connected to a calibrated pressure gauge by a short piece of tubing. Prior to each session of data collection the pressure gauge was zeroed by placing a column of water at the centerline of the pipe and setting the gauge at zero. Pressure measurements for each test run were read directly from the gauge. Ranges of pressure obtained from pressure gauge measurement were always within the limits of the instrumentation. Maximum pressure was always well below the upper limits of the gauge and the minimum pressure was set at a point that ensured pressurized flow in the conduit.

Downstream air pressure

The downstream air pressure was measured to determine the efficiency of the air vent. Literature suggests that large negative pressures can form at or near the air vent if head loss is excessive, however a sufficiently large diameter air vent could maintain pressures close to atmospheric pressure (Ghetti and Di Silvio, 1967).

A manometer filled with water was used to determine the air pressure in the area above the water surface immediately downstream of the control gate. Figure 9 shows the manometer and general setup that was used; the pressure tap location was previously

shown in Figure 5. One side of the manometer was connected to the pressure tap located downstream of the gate using a short length of tubing, while other side was open to atmospheric pressure. Pressure inside to the conduit was determined by measuring the water differential on the manometer with a ruler.

There was some uncertainty regarding the accuracy of the measurements obtained from the water manometer and the integrity of the pressure tap. One potential source of error deals with the location of the pressure tap and its impact on the measurement of pressure on a water manometer. Although there was some uncertainty relating to this measurement, all measured pressures were well within the limits of the system used in measurement.

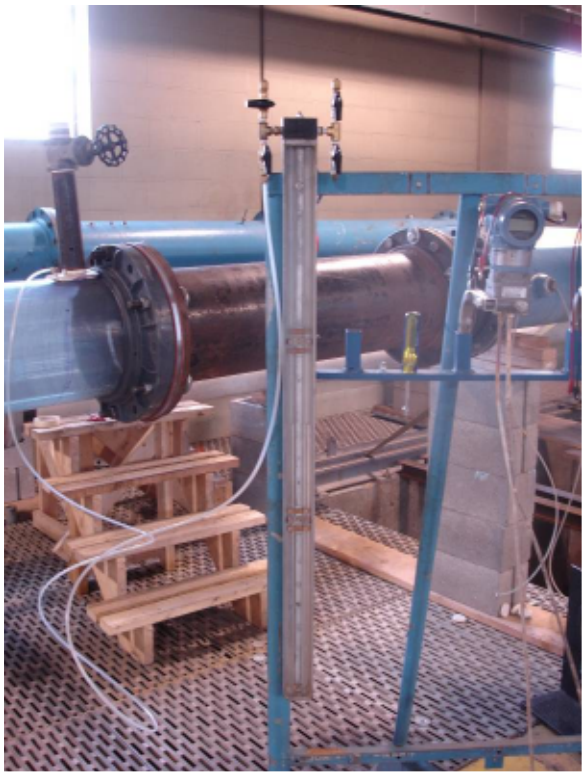

Figure 9. Manometer used to determine air pressure.

Air flow rate

Air velocity rate was measured directly in the air intake piping and was used to determine the air flow rate. The air velocity rate was determined by using a Dwyer series 471 digital thermo velocity probe shown in Figure 10. This measurement was accomplished by inserting the air velocity probe into the 0.375-in diameter hole on the side of the air intake piping, so that the probe sensor was located at the center of the air intake pipe. Each air demand measurement was taken over a period of 30 sec or longer in order to ensure that the air velocity reading from the probe had sufficient time to stabilize. A maximum and minimum reading were recorded from which the average air demand was calculated. After obtaining a value of the air velocity an air demand flow

Figure 10. Air velocity probe.

rate through the air vent was calculated assuming that the cross-sectional velocity profile in the air intake pipe was uniform. This assumption was verified simply by placing the air velocity probe at different locations inside of the air intake.

The air velocity probe used for air velocity measurements was accurate to ± 3 percent. Care was taken to ensure that the velocity sensor on the probe was always perpendicular to the direction of flow in the pipe to provide the most accurate measurements possible.

Air velocity profile

The air velocity profile inside the conduit was measured in an effort to define the characteristics of the air mass above the free water surface. The air velocity was measured by inserting the air velocity probe into the 0.375-in diameter hole in each rubber stopper located at 10-ft intervals along the crown of the conduit (see Figure 11). Air velocity data at three points at each measurement location were obtained, with the first being a distance of 0.25-in from the roof of the conduit, the second being from 2.5-in to 3.5-in from the water surface, and the third being half way in between the two. A cross-sectional view of the conduit and typical air velocity profile measurement locations is shown Figure 12. The air velocity probe was left inside the conduit for approximately 30 sec for the reading to stabilize so that the average air velocity could be determined at each point.

Figure 11. Air velocity profile measurement.

The air velocity probe was subject to several uncertainties and limitations. It would not give accurate results when it came in contact with water droplets. For this reason, it was not feasible to obtain air velocity profile measurements below the lowest defined point. Due to excessive water droplets above the water surface, it was impossible to obtain any air velocity profile measurements for some test runs with large amount of spray or water droplets. Another limitation of the device was its inability to measure velocity direction. This became a significant problem when measuring the air velocity in opaque PVC pipe sections, many velocity measurements were obtained with no idea of an associated direction.

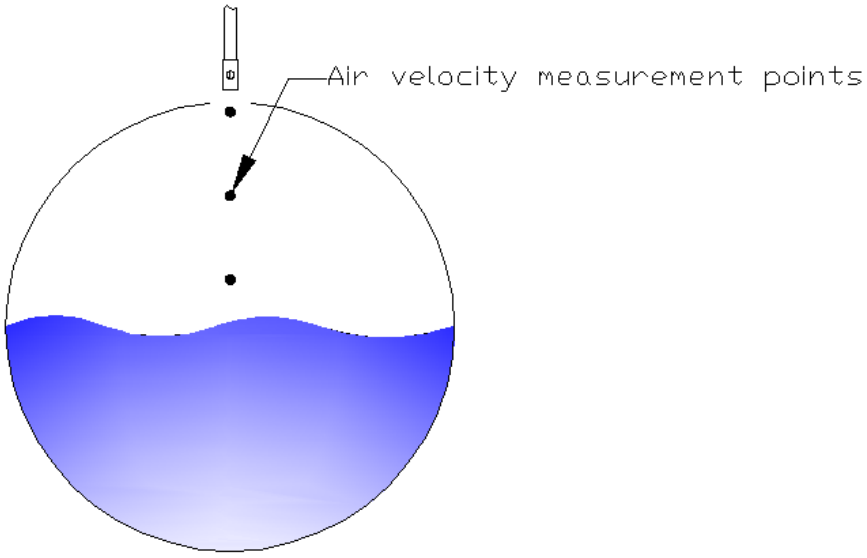

Figure 12. Conduit cross-section and air velocity measurements.

Figure 13. Depth and water surface depth measurement.

Water surface and roughness depth

Water surface depth was measured in order to aid in the analysis of the air demand ratio data and was used in Froude number calculations. Water depth was measured at each hole along the crown of the conduit by using a steel ruler with a point gauge on one end (see Figure 13). The water depth was found by subtracting the measurement from the inside diameter of the conduit. Water depth was measured and defined as the point where the point gauge was half way in between the top of all waves and significant spray and the bottom of the water surface waves where it the gauge would become completely submerged as shown in Figure 14.

The turbulent water surface roughness was measured in order to determine the effects of water surface roughness on air demand. It was measured by placing the point gauge at the elevation where it first came in contact with waves or spray from the main mass of water (see Figure 14).

It was often difficult to ensure that the point gauge was at the proper elevation for water depth and surface roughness measurements due to poor visualization. A flashlight was employed to illuminate the water surface through the hole, but this often made the situation worse by blocking light completely to the entire hole. Highly turbulent flows also provided a challenge to accurately measure due to the amount of spray that came out of the hole when the point gauge was touching the water surface.

End cap placement

The location or depth of the end cap was determined similar to the water depth and surface water roughness. When the end cap was utilized, it was lowered to a point

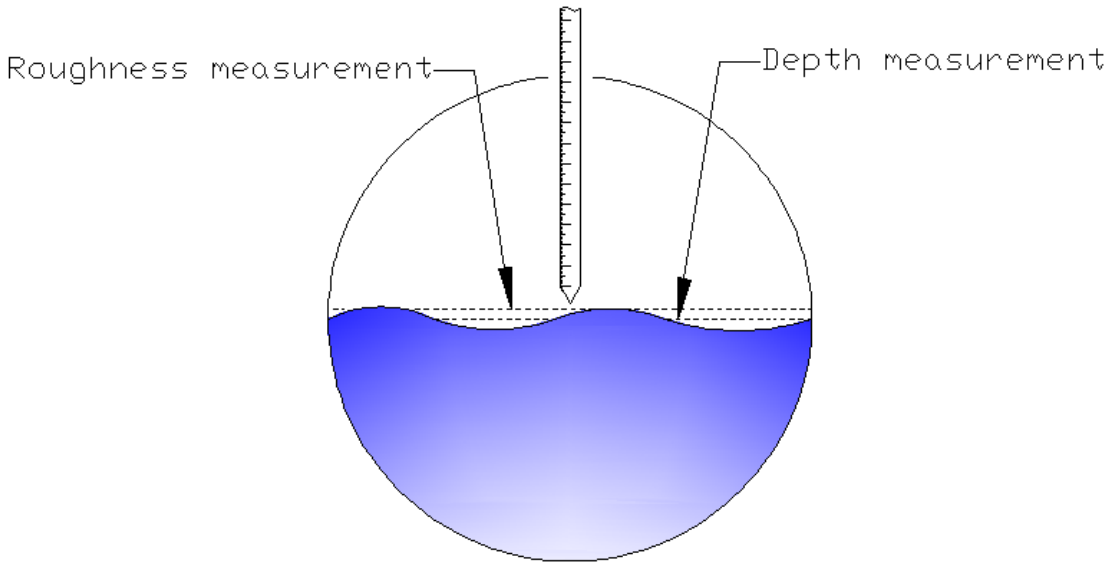

Figure 14. Conduit cross-section with water depth and surface roughness measurements.

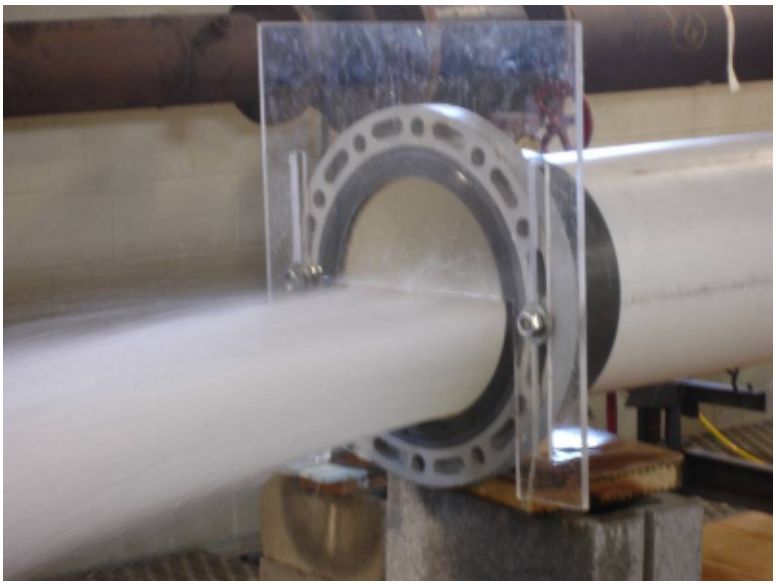

Figure 15. Placement of end cap.

where it was just touching the water surface but not affecting the water flow. If the gate was too low, it would cause a hydraulic jump to move up the pipe and eventually pressurize the conduit. When the end cap was placed properly, it would barely skim the upper portion of the water surface roughness as shown in Figure 15.

Data Collection

All experimental setups used throughout the study are shown in Table 1. Conduit slope was set at either 2.5 percent or 0.15 percent for every test run. Data was collected for two different conduit lengths, 48 ft and 29 ft. A range of gate openings were tested from 10 to 90 percent cross-sectional area, including one gate at 50 percent with a serrated gate bottom (see Figure 4). Tests were executed both with and without the acrylic end cap in place for a range of flows, gate openings, and slopes.

Air demand data for each configuration and test run are shown in Appendix B. All test data was obtained through a simple procedure. The first step for data collection involved setting and recording a desired flow rate. As many as three discharges were recorded for each test configuration. The first discharge corresponded with the maximum discharge available in the laboratory supply line. The second discharge corresponded to the condition that would keep the upstream supply pipe fully pressurized; this pressure was determined to be close to 0.25 psi at the upstream pressure tap. The third discharge was typically the average flow rate from the first two discharges. However, data for three discharges at each test setup were often infeasible due to laboratory scheduling and only one or two discharges were tested. Once the discharge and pressure upstream of the

Table 1. Outline of physical model configurations

Setup	Test	Conduit Slope	Conduit Length	Gate Opening	End Cap in Place
1	1A, 1B, 1C	2.50%	48 ft	90%	No
2	2A, 2B, 2C	2.50%	48 ft	70%	No
3	3B	2.50%	48 ft	70%	Yes
4	4A, 4B, 4C	2.50%	48 ft	50%	No
5	5A, 5B	2.50%	48 ft	50%	Yes
6	6A, 6B	2.50%	29 ft	50%	No
7	7A, 7B	2.50%	29 ft	50%	Yes
8	8A, 8B	2.50%	48 ft	50% Rough	No
9	9A, 9B	2.50%	48 ft	50% Rough	Yes
10	10A, 10B	2.50%	29 ft	50% Rough	No
11	11A, 11B	2.50%	29 ft	50% Rough	Yes
12	12A, 12B, 12C	2.50%	48 ft	30%	No
13	13B	2.50%	48 ft	10%	No
14	14B	2.50%	48 ft	10%	Yes
15	15A, 15B, 15C	0.15%	48 ft	70%	No
16	16A, 16B, 16C	0.15%	48 ft	70%	Yes
17	17A, 17B, 17C	0.15%	48 ft	50%	No
18	18A, 18B, 18C	0.15%	48 ft	50%	Yes
19	19A, 19B	0.15%	29 ft	50%	No
20	20A, 20B	0.15%	29 ft	50%	Yes
21	21A, 21B, 21C	0.15%	48 ft	50% Rough	No
22	22A, 22B, 22C	0.15%	48 ft	50% Rough	Yes
23	23A, 23B	0.15%	29 ft	50% Rough	No
24	24A, 24B	0.15%	29 ft	50% Rough	Yes
25	25A, 25B, 25C	0.15%	48 ft	30%	No
26	26A, 26B, 26C	0.15%	48 ft	30%	Yes
27	27B	0.15%	48 ft	10%	No
28	27B	0.15%	48 ft	10%	Yes

control gate were set to the desired values, all other measurements previously defined were obtained. Air velocity profile measurements were conducted for only a 2.5 percent conduit slope and length of 48 ft. Air velocity profile data is shown in Appendix C.

Additionally, to single out the effects of each variable, it was desired to keep as many physical parameters as constant as possible, while varying one variable at a time. For this reason, many model tests were conducted at a common gate opening of 50 percent. This gate opening was chosen because it yielded the largest amount of air demand out of all preliminary testing.

Some air velocity profile and air flow rate observations were made through the use of a smoke source. Smoke was forced in several holes along the crown of the conduit and in the air intake piping. Air turbulence and flow patterns were observed and recorded in the clear section of 12-in diameter PVC directly downstream of the control gate and the exit portal of the conduit.

CHAPTER 4

EXPERIMENTAL RESULTS

Introduction

This chapter includes a discussion of the experimental results and shows graphical results for each test condition. An outline of all setups and tests runs is shown in Table 1. Data for each setup and individual test run are shown in Appendix B. All calculations for all ratios and parameters utilized in the following plots have been previously defined. The effects of each model variable on air demand will be based on the head to gate ratio or Froude number. Model variables discussed include: end cap use, gate opening, gate and water surface roughness, conduit slope, and conduit length. Observations regarding flow depth and the velocity profile in the conduit are also discussed.

Results

Total upstream energy head was altered for each test run in order to obtain data for three or two flow rates for almost every model configuration. The downstream air pressure measured for each test run and model configuration indicated that the pressure inside of the conduit was always very close to atmospheric pressure. Therefore it can be assumed that air intake pipe was not undersized and did not cause excessive head loss. The relationship between the measured air-demand ratio and head-to-gate ratio typically provided reasonable results. When there were no significant conduit geometry changes between runs, a linear relationship between the air-demand ratio and head-to-gate ratio

existed. The relationship between air demand and Froude number also provided reasonable results and was best described using a second order polynomial fit. The general relationship between air demand and the Froude number for all free surface data points is shown in Figure 16.

End cap

In order to determine the portion of the air demand that was entrained into the water, identical tests with and without the end cap were conducted. All tests used to determine the portion of air entrained in the fluid are shown in Table 2. It was assumed that the difference between air demand for identical runs with and without the end cap

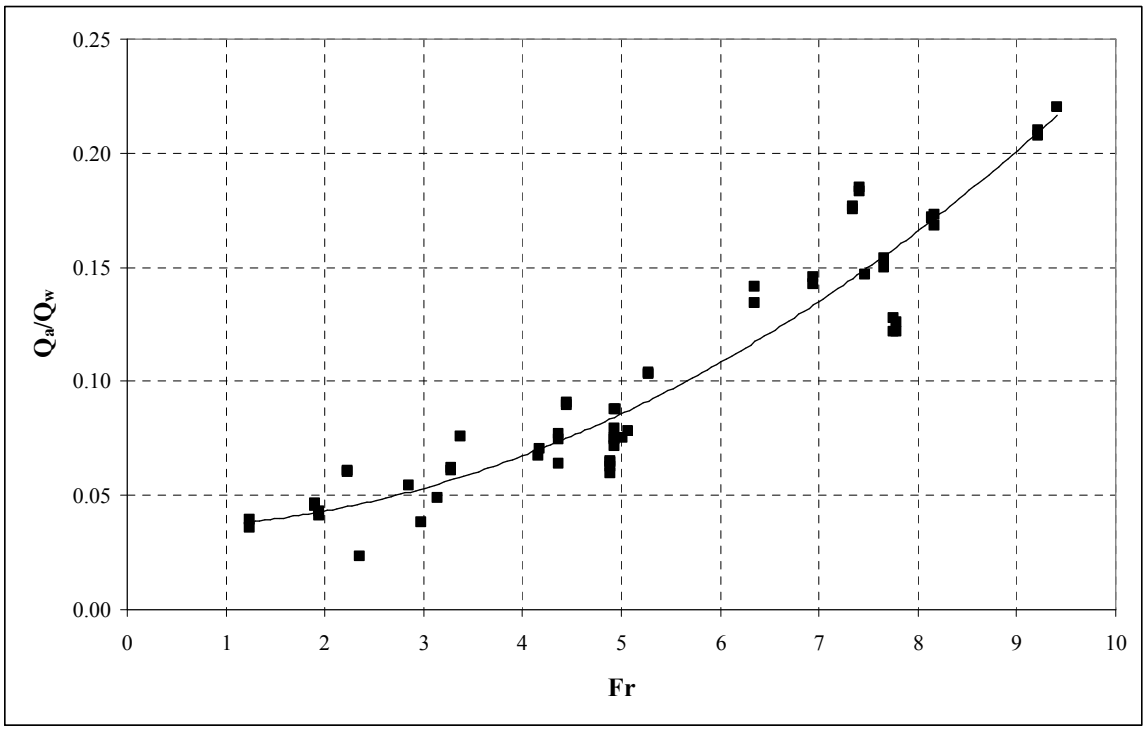

Figure 16. Plot of air demand ratio and Froude number for all data.

would represent the amount of air entrained into the liquid. This assumption was based on the hypothesis that there would be no shift in the mechanism of a demand between runs with and without the end cap and when the end cap was lowered there would be no significant way for air to escape the conduit unless it became entrained in the water.

Figure 17 shows a plot of the air demand ratio in relation to Froude number for test configurations with and without the end cap. As can be seen in this figure, there was essentially no difference between the air demand measured in the air intake with and without the end cap in place. Figure 18 shows the effect of the end cap on the air demand ratio and head to gate ratio for two identical runs for model setups 17 and 18. Again, it is evident that there was no significant difference in the air demand for tests ran with and without the end cap in place. Due to the number of identical test runs with and without the end cap, it can be confidently stated that most of the air demand in the system can be attributed to air entrainment rather than air flow above the water.

Table 2. List of setups used for end cap study

Setup	Test	Conduit Slope	Conduit Length	Gate Opening	End Cap in Place
2	2B	2.50%	48 ft	70%	No
3	3B	2.50%	48 ft	70%	Yes
4	4A, 4B	2.50%	48 ft	50%	No
5	5A, 5B	2.50%	48 ft	50%	Yes
15	15A, 15B, 15C	0.15%	48 ft	70%	No
16	16A, 16B, 16C	0.15%	48 ft	70%	Yes
17	17A, 17B, 17C	0.15%	48 ft	50%	No
18	18A, 18B, 18C	0.15%	48 ft	50%	Yes
25	25A, 25B, 25C	0.15%	48 ft	30%	No
26	26A, 26B, 26C	0.15%	48 ft	30%	Yes

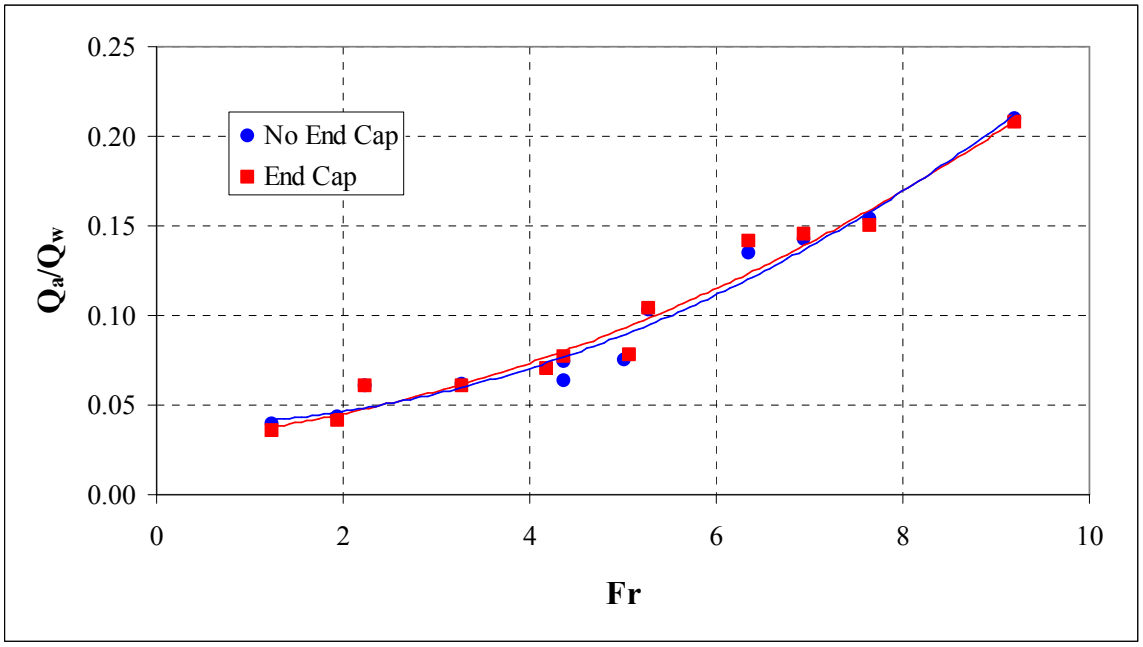

Figure 17. Plot of air demand ratio and Froude number for data for end cap comparison.

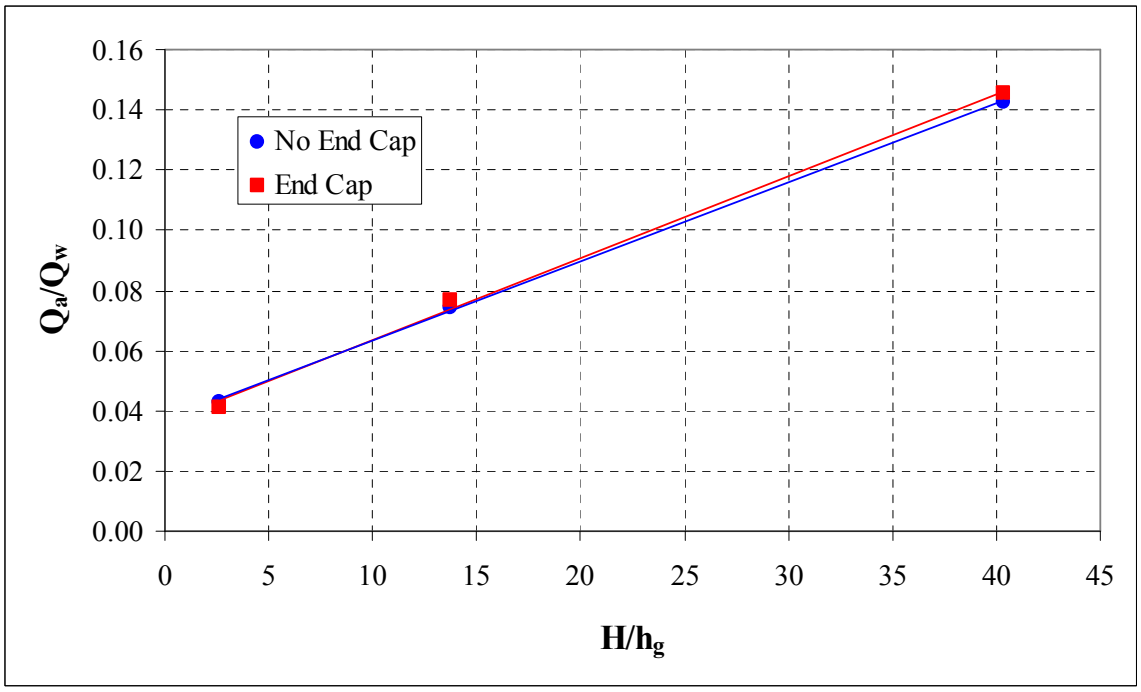

Figure 18. Plot of air demand ratio and head to gate ratio for setups 17 and 18.

Gate opening

In order to determine the effect of gate opening on air demand, the relationship between the air demand ratio and the head to gate ratio were plotted in Figure 19 for different gate openings. This plot illustrates that the slope of the curve for the air demand ratio and head to gate ratio changes with respect to gate opening. The slope of each gate opening curve was determined by calculating the mean slope of all tests outlined in Table 3. A tabular list of the slope of each gate opening with its associated standard deviation is listed in Table 4. Of course, the slope of the linear relationship between the air-demand ratio and head-to-gate ratio only holds true when all other parameters are held constant. Modifying gate roughness, water surface roughness, and conduit length all had significant impacts on the slope of the curve found, while conduit slope did not show a

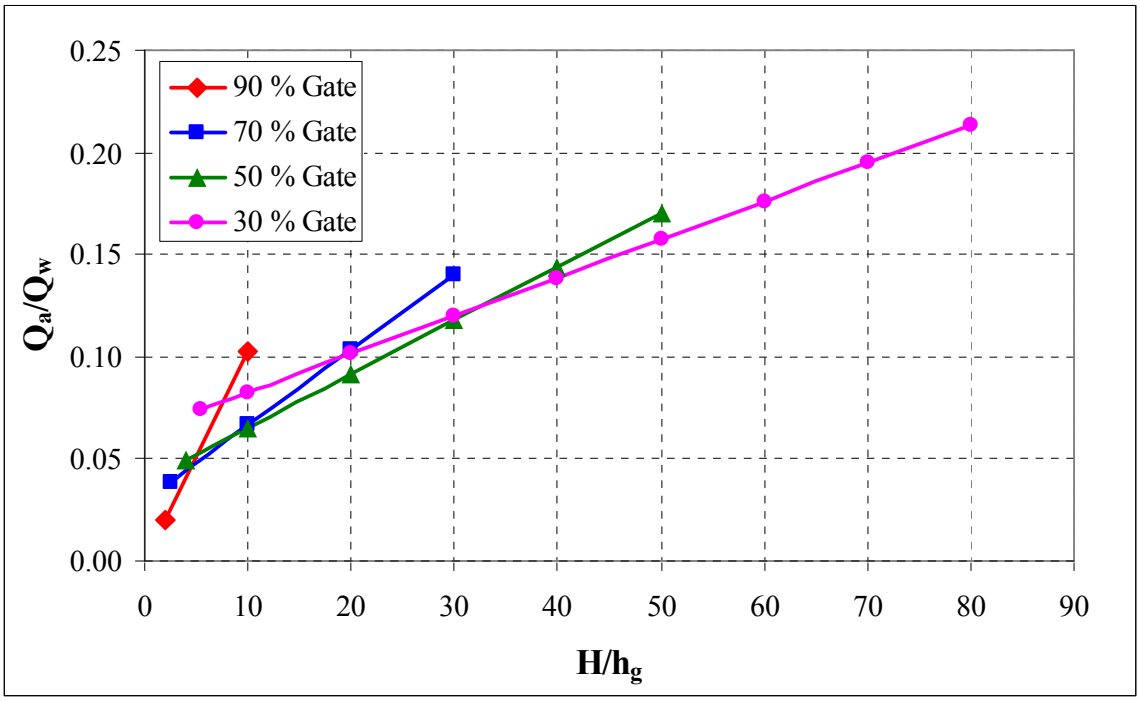

Figure 19. Plot of air demand ratio and head to gate ratio for gate opening.

Table 3. List of setups used for gate opening comparison

Setup	Test	Conduit Slope %	Conduit Length	Gate Opening	End Cap in Place
1	1A, 1B, 1C	2.50%	48 ft	90%	No
2	2A, 2B, 2C	2.50%	48 ft	70%	No
4	4A, 4B, 4C	2.50%	48 ft	50%	No
5	5A, 5B	2.50%	48 ft	50%	Yes
12	12A, 12B, 12C	2.50%	48 ft	30%	No
15	15A, 15B, 15C	0.15%	48 ft	70%	No
16	16A, 16B, 16C	0.15%	48 ft	70%	Yes
17	17A, 17B, 17C	0.15%	48 ft	50%	No
18	18A, 18B, 18C	0.15%	48 ft	50%	Yes
25	25A, 25B, 25C	0.15%	48 ft	30%	No
26	26A, 26B, 26C	0.15%	48 ft	30%	Yes

Table 4. Slope of gate opening curves

Gate Opening	Setup	Average Slope	Standard Deviation
90%	1	0.01040	-
70%	2, 15, 16	0.00370	0.000100
50%	4, 5, 17, 18	0.00263	0.000050
30%	12, 25, 26	0.00187	0.000058

significant difference.

In Figure 19 it is evident that the air-demand ratio for the minimum head to gate ratios are within the same range of magnitude for each gate while the air-demand ratio for maximum head to gate opening ratio was significantly lower for the larger gates. This occurred because the available water pressure in the laboratory was limited. Thus, it was possible to obtain data for small values of the head to gate ratio for all gate openings, but sufficient pressure was not available to achieve higher head to gate ratios for large gate openings.

Gate and water surface roughness

In order to determine the effect of water surface roughness on the air demand ratio, an artificially rough gate was installed which would increase the surface roughness of the air-water interface. Only one serrated gate was fabricated; a 50 percent gate opening was chosen because it demonstrated the maximum air demand ratio possible based on the maximum laboratory pressure (see Figure 4). The serrated 50 percent gate had an identical rating curve as the smooth 50 percent gate due to the fact that the average gate height and area opening were identical between the two gates. All data used for this comparison is listed in Table 5. Figure 20 shows a plot of the air demand ratio and head to gate ratio for the smooth and rough gate. There is a clear difference between the line represented by the rough gate and the smooth gate of the same opening. It is clear that gate roughness and subsequently the water surface roughness causes a significant increase on the air demand ratio between these two identical tests.

In Figure 21 the air demand ratio is plotted against the average water surface roughness along the entire conduit (R_w); it can also be observed that there is a relationship between the air demand ratio and the water surface roughness. Although, it is interesting to point out that the same air demand was measured for runs with significantly different water surface roughness for the first set of points in Figure 20 and Figure 21. This could be due to the fact that at slower velocities the water surface roughness was largely due to wave action, while at larger velocities water surface roughness was more turbulent and involved spray. Figure 21 shows a plot between the

surface water roughness and head to gate ratio. It is evident that the rough gate creates a larger water surface roughness for the same head-to-gate ratio as the smooth gate.

Table 5. Data in determining the effects of gate roughness on air demand

Setup	Test	Conduit Slope	Conduit Length	Gate Opening	End Cap in Place
4	4A, 4B, 4C	2.50%	48 ft	50%	No
5	5A, 5B	2.50%	48 ft	50%	Yes
8	8A, 8B	2.50%	48 ft	50% Rough	No
9	9A, 9B	2.50%	48 ft	50% Rough	Yes
17	17A, 17B, 17C	0.15%	48 ft	50%	No
18	18A, 18B, 18C	0.15%	48 ft	50%	Yes
21	21A, 21B, 21C	0.15%	48 ft	50% Rough	No
22	22A, 22B, 22C	0.15%	48 ft	50% Rough	Yes

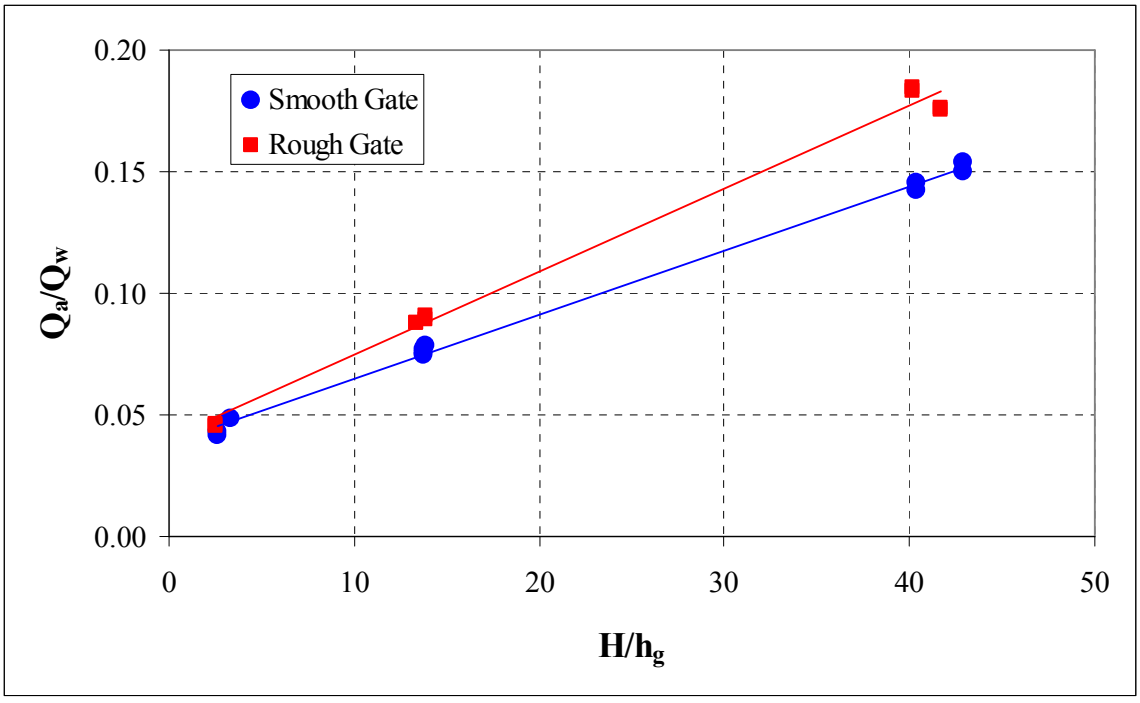

Figure 20. Plot of air demand ratio and head to gate ratio for gate roughness.

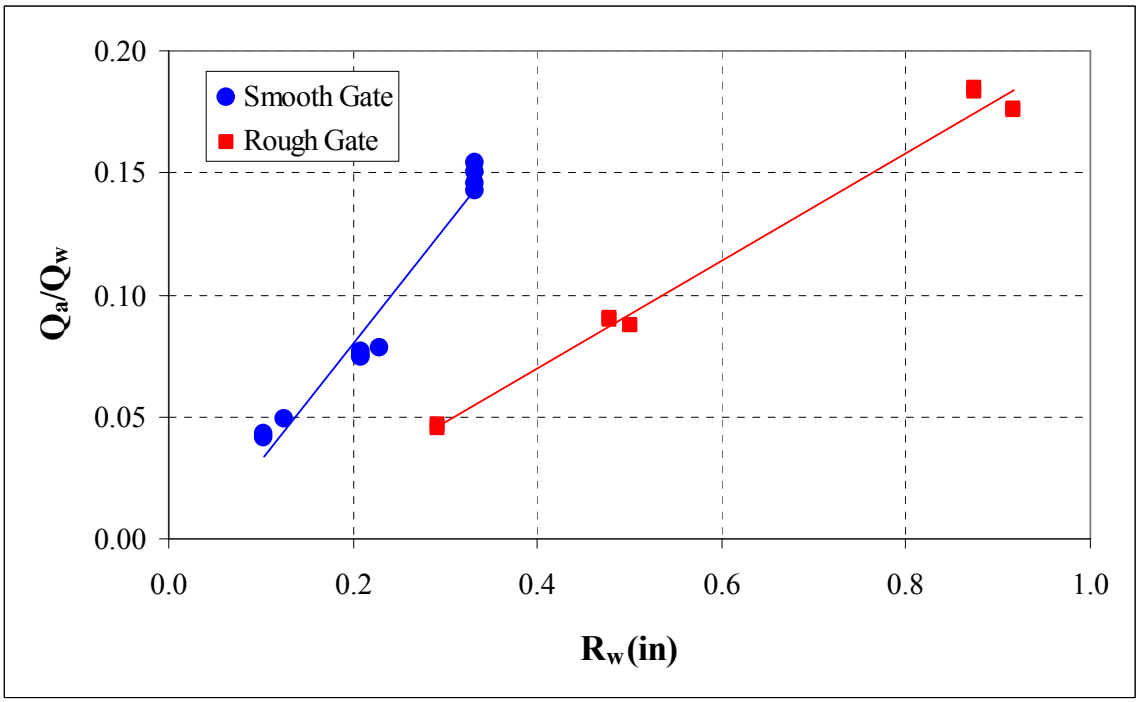

Figure 21. Plot of air demand ratio and water surface roughness.

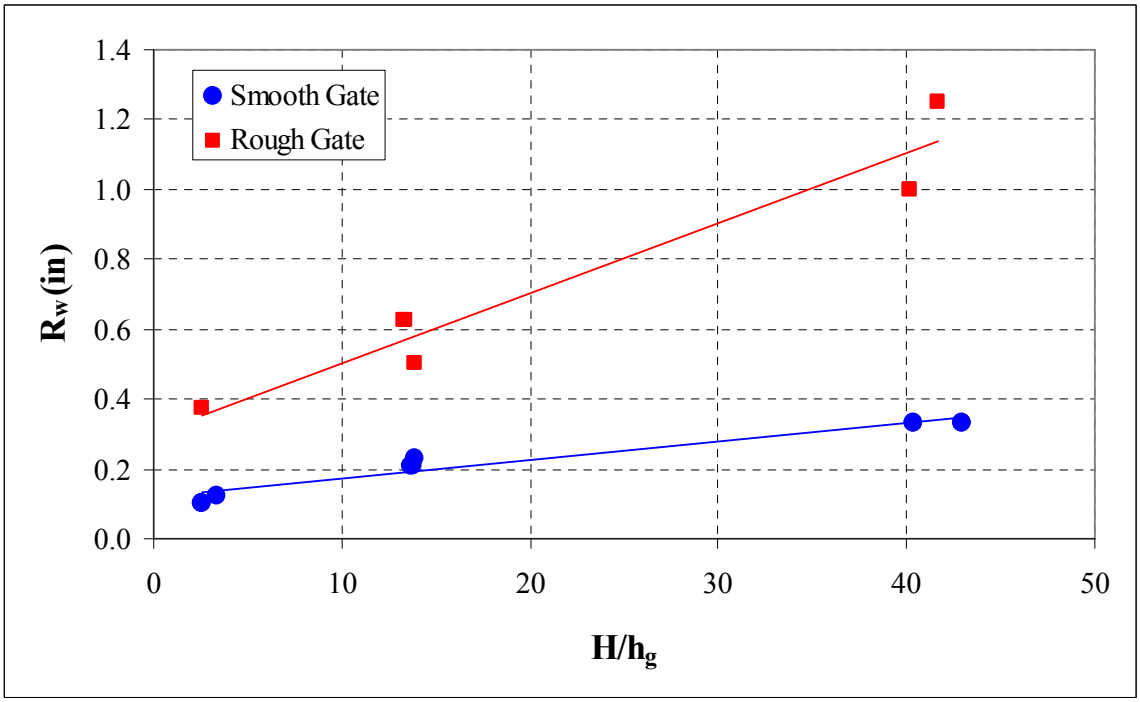

Figure 22. Plot of water surface roughness and gate to head ratio.

Table 6. Test data used in comparison of conduit slope on air demand

Setup	Test	Conduit Slope	Conduit Length	Gate Opening	End Cap in Place
2	2A, 2B, 2C	2.50%	48 ft	70%	No
4	4A, 4B, 4C	2.50%	48 ft	50%	No
5	5A, 5B	2.50%	48 ft	50%	Yes
12	12A, 12B, 12C	2.50%	48 ft	30%	No
15	15A, 15B, 15C	0.15%	48 ft	70%	No
17	17A, 17B, 17C	0.15%	48 ft	50%	No
18	18A, 18B, 18C	0.15%	48 ft	50%	Yes
25	25A, 25B, 25C	0.15%	48 ft	30%	No

Conduit slope

In order to test the effect of slope on air demand the downstream conduit slope was altered between 2.5 percent or 0.15 percent. Identical tests were conducted with both slopes to aid in the comparison. A list of all test data used is listed in Table 6. Figure 23 shows a plot of the air demand ratio and Froude number for all tests listed in Table 6. Notice at the low end of the curves that the 2.5 percent slope receives the same amount of air as the 0.15 percent slope at different Froude numbers. This is due to the fact that the air-demand ratio is for each run is almost identical but the slope of the conduit causes the water depth in the conduit to change. Because the 0.15 percent slope produces larger water depths and slower water velocities than the 0.25 percent slope the Froude number is smaller for runs that would otherwise be identical. Figure 24 shows a plot of the air-demand ratio and the head-to-gate ratio for each conduit slope; notice that there is essentially no difference between the air demand of the two slopes. Although there is no apparent effect of slope on air demand, it is important to note that most methods for

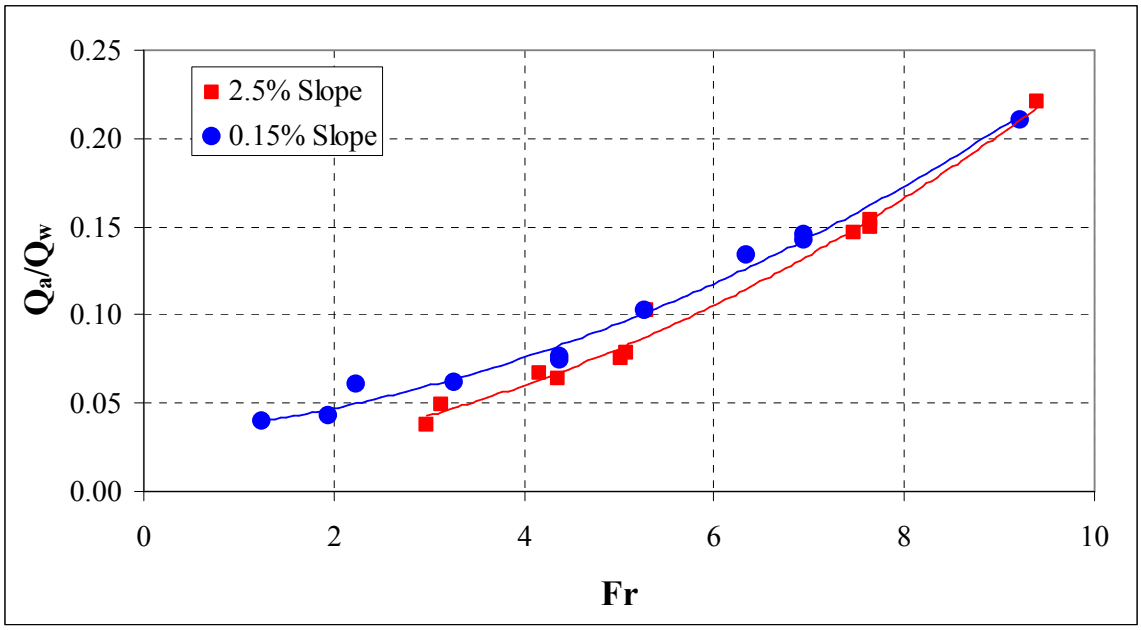

Figure 23. Plot of air demand ratio and Froude number for differing slopes.

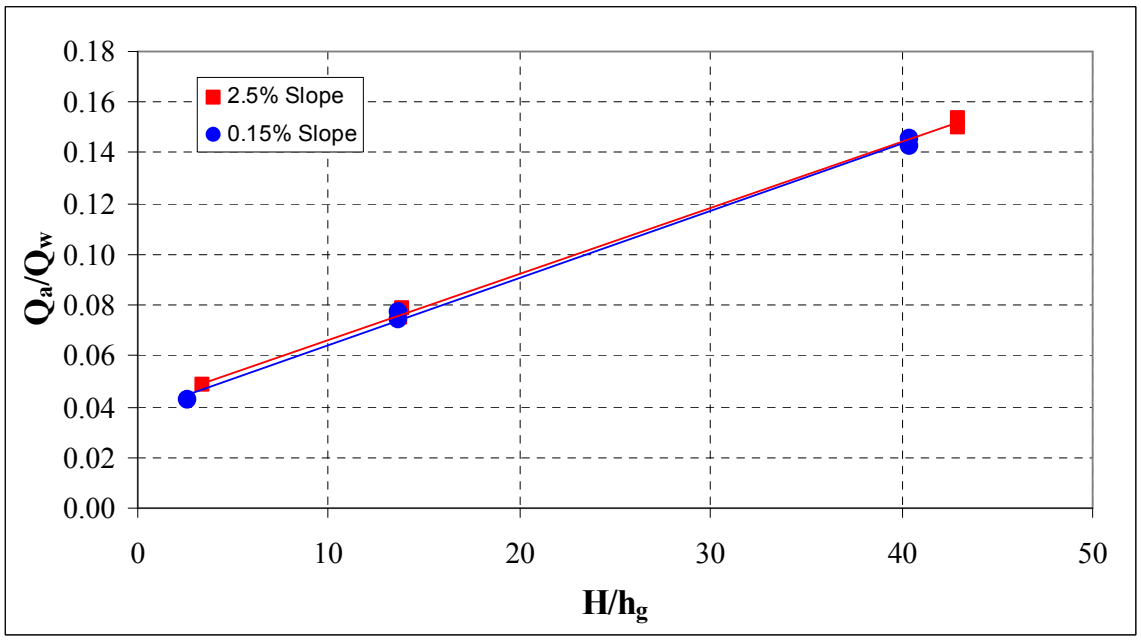

Figure 24. Plot of air demand ratio and head to gate ratio for differing slopes

estimating air demand are based on the Froude number. For this reason the Froude number is not an adequate means of comparing the air-demand ratio between conduits of different slopes.

Effect of conduit length on air demand

Table 7 outlines tests that were used to determine the effect of conduit length on the air demand ratio. Figure 25 shows the relationship of air demand ratio and head to gate ratio for different conduit lengths. It is clear from the plot that there is more air demand at the air intake for the 48 ft conduit length. It is interesting to note that the difference in air demand between the two conduit lengths is not proportional to the decrease in conduit length. The air demand ratio is decreased by an average of 20 percent while the conduit length is decreased by 40 percent. This indicates that a larger portion of air demand from the vent is being entrained near the beginning of the conduit.

Air velocity profile discussion

Air velocity profile measurements were conducted for many test runs at a slope of 2.5 percent. Appendix C contains all data that was obtained for the conduit velocity profile measurements. Note that the air probe was used only to measure the magnitude of the air velocity and not the direction. Air velocity direction was assigned when possible, but a majority of points taken were lacking a direction. The clear PVC conduit section and exit portal provided reasonable results for air velocity direction based on visualization with the aid of a smoke source. It was found that air was often traveling upstream at the crown of the conduit, and was traveling downstream near the water

Table 7. Data used for length comparison

Setup	Test	Conduit Slope	Conduit Length	Gate Opening	End Cap in Place
4	4A, 4B	2.50%	48 ft	50%	No
5	5A, 5B	2.50%	48 ft	50%	Yes
6	6A, 6B	2.50%	29 ft	50%	No
7	7A, 7B	2.50%	29 ft	50%	Yes
8	8A, 8B	2.50%	48 ft	50% Rough	No
9	9A, 9B	2.50%	48 ft	50% Rough	Yes
10	10A, 10B	2.50%	29 ft	50% Rough	No
11	11A, 11B	2.50%	29 ft	50% Rough	Yes
17	17A, 17B	0.15%	48 ft	50%	No
18	18A, 18B	0.15%	48 ft	50%	Yes
19	19A, 19B	0.15%	29 ft	50%	No
20	20A, 20B	0.15%	29 ft	50%	Yes
21	21A, 21B	0.15%	48 ft	50% Rough	No
22	22A, 22B	0.15%	48 ft	50% Rough	Yes
23	23A, 23B	0.15%	29 ft	50% Rough	No
24	24A, 24B	0.15%	29 ft	50% Rough	Yes

surface. This observation was difficult to confirm in conduit sections that did not provide flow visualization. Velocity measurements provided little insight due to the lack of velocity direction at each point.

Smoke source tests were conducted for model configurations 4 and 6. Smoke was placed in the air intake for test run 8 (50 percent gate opening at 2.5 percent slope and conduit length of 48 ft); the exit portal of the conduit was observed to have a very small amount of smoke exit in a very non-uniform puffing at a much slower velocity magnitude then the water exiting the conduit. An identical smoke bomb test was done for test run 32 (50 percent gate opening at 2.5 percent slope and conduit length of 29 ft), a slightly larger

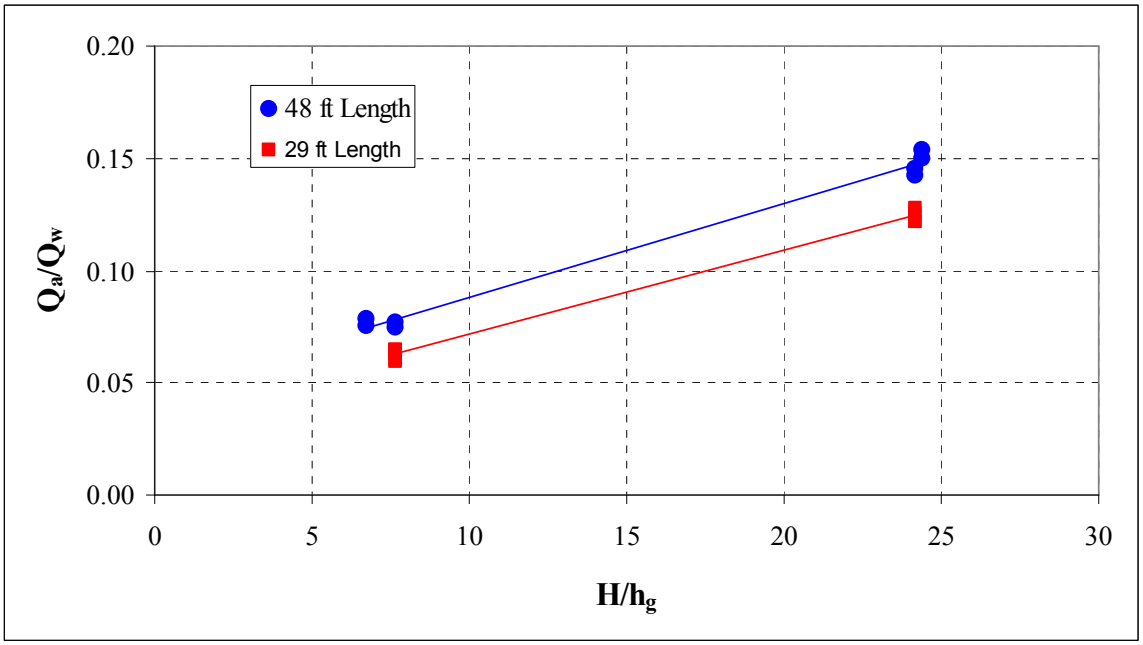

Figure 25. Plot of air demand ratio and head to gate ratio for smooth gate.

portion of smoke was seen exiting the conduit. For the same test runs a smoke bomb was then suspended from the measurement hole closest to the air intake piping. Smoke was clearly observed traveling upstream along the crown of the pipe and then reversing flow in a significant eddy and then dissipating near the air-water interface near the air vent. Identical behavior was observed for both tests 8 and 32.

From these results there is evidence that the air velocity profile described by Campbell and Guyton (1953), Sikora (1967) as cited in Falvey (1980), and Falvey (1980) are not a significant driving factor in producing air demand in this experimental setup. This evidence can also be verified through the use of the end cap, which showed that most if not all of the air demand was due to air entrainment in the conduit.

CHAPTER 5

DATA ANALYSIS

There has been little published data on the relationship between the physical characteristics of conduit geometry and air demand. Suffice it to say that most researchers have combined large amounts of prototype and model data together, sometimes with a significant amount scatter, and developed general empirical relationships based on the Froude number. They have not considered some of the geometric changes discussed in this research. Despite the lack of similar test results, to have confidence in this study general air demand results will be compared to methods listed in the literature.

The air demand ratio has been found to be somewhat dependent on the Froude number of the flow. It has been found that the air demand required for a hydraulic jump flow that fills the conduit given by Kalinske and Robertson (1953) in Equation (1) can represent a minimum value of air demand in free surface flow (Ghetti and Di Silvio, 1967). A theoretical maximum value of air demand may be described as the air entrainment in a completely open channel or spillway, Equation (7) as illustrated by Falvey (1980) represents the amount of air entrained in a spillway. This comparison is shown in Figure 26, and shows that the air demand data for this research fell within the limits defined for free surface flow. This plot also suggests that free surface air demand in a closed conduit is more closely related to a hydraulic jump condition than to open channel air entrainment.

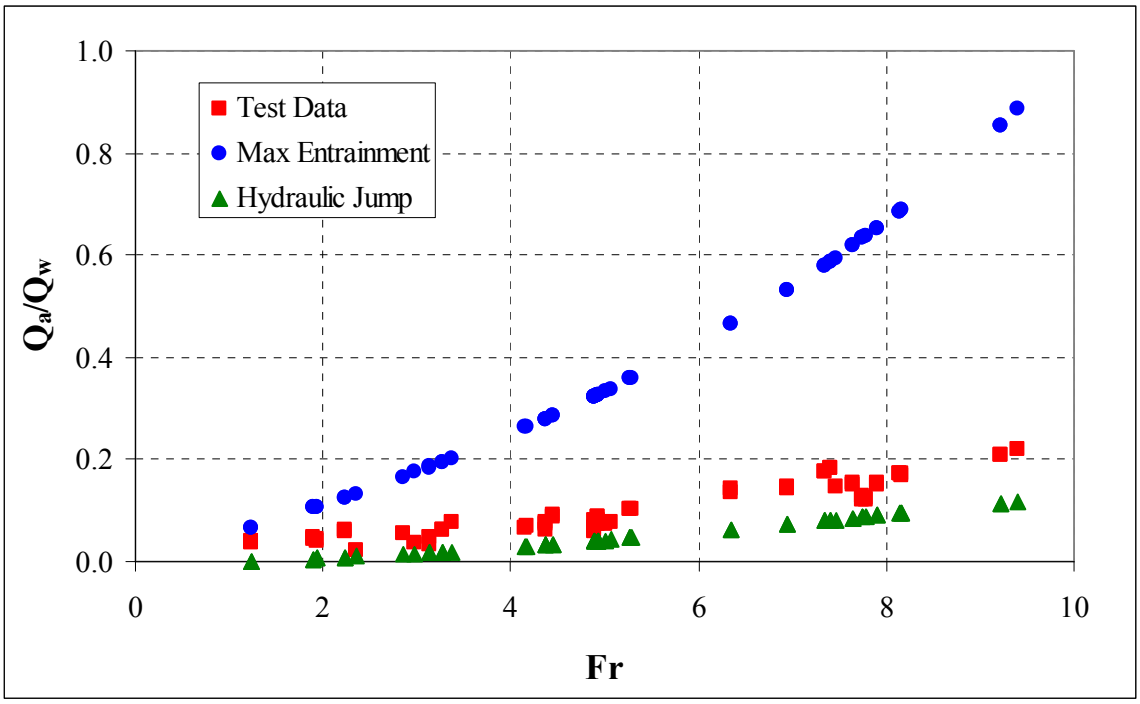

Figure 26. Plot of entrainment limits for air demand.

Test data for this study were also compared to Froude number based estimates given by previous researchers. In Figure 27 measured air data is compared to the Froude number based empirical equations of Equations (3) and (11) given by the USACE (1964) and Winser (1967) as cited in Sharma (1976), respectively. The difference between the curve defined by Sharma and the others can be explained through the fact that Sharma's curve was developed as an upper limit envelope curve for large amounts of prototype and model data that may have been influenced by large variations in physical characteristics. Data obtained for the present study was similar but slightly lower than estimated values of air demand for curves defined by USACE and Winser. It is important to point out that air demand curves shown in Figure 27 were also empirically developed based on large amounts of prototype and model data, and similar to Sharma (1976) create conservative

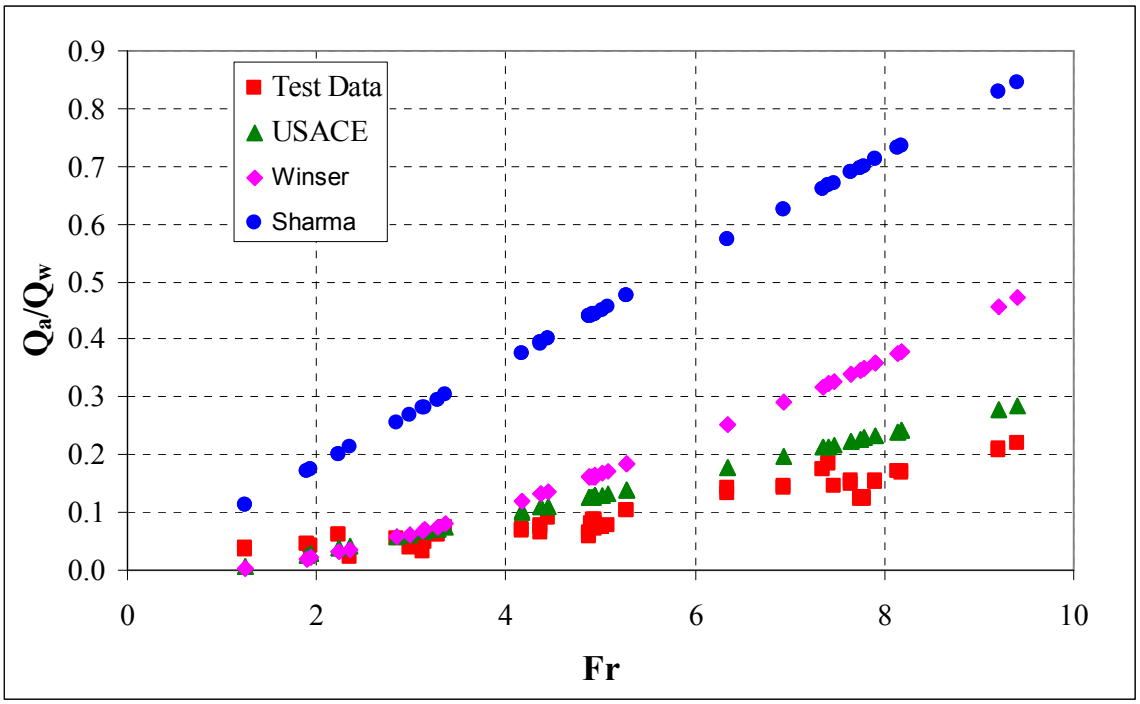

Figure 27. Plot of air demand comparisons from literature.

estimates for air demand.

Air velocity profile methods described in the literature do not seem to be accurate for this research. This could be predominately due to the fact that these methods assume a large amount of air traveling above the water surface; this was not the case in this study. Take, for example, the method given by Sikora (1967) as cited in Falvey (1980), which assumed that the air mass was traveling at a speed equal to the water surface velocity. When the maximum water surface drops below half of the conduit height the air demand ratio would have a value above one and would continue to increase until there was no water running in the conduit. In addition to the author's observations, Sharma (1976) also found that a defined air velocity profile above the water surface did not simulate real conditions.

Test results in this study suggest that almost all air demand that was measured in the air vent was entrained into the fluid. These findings are relatively consistent with those of Speerli and Hager (2000) who determined that a significant amount of the air demand was entrained into the fluid. Speerli (1999) found that the total air discharge, the sum of the air demand at the air intake and air entering the downstream conduit, is independent of air vent head loss. In cases when the air vent created excessive head loss, it was found that the air demand came from the downstream end of the conduit to provide the same total amount of air to be entrained in the fluid. This could suggest that there is a certain amount of air entrainment that must be satisfied, after which no additional air demand is drawn into the fluid.

The results that shortening the length of the conduit actually caused a decrease in air demand measured from the air vent can be verified through the findings of Speerli (1999). It was found that when conduit length was decreased a decrease in the air entering the conduit from the upstream air vent occurred. This could be because the amount of air entering through the exit portal of the conduit increased. It should be noted that the decrease in air demand was not proportional to the decrease in length. This could be because a larger amount of air is entrained in the beginning section of conduit downstream of the gate as shown by Speerli and Hager (2000).

CHAPTER 6

CONCLUSIONS

In summary, this research presents an analysis of air demand in closed gated conduits for free surface flow. Background was provided which outlines the use of gated closed conduits and their importance and relevance in engineering practice. A thorough literature review was conducted which presented the current methods that are used to estimate air demand in closed gated conduits. The theory used in presenting the results and conducting this laboratory experiment are explained in detail. The physical experiment, measurements required, and data collection has been discussed in great detail. Results and findings have been discussed. The data obtained in this research have been compared to methods available in literature.

The following conclusions can be made from this study:

1. The use of the Froude number can be used to describe air demand in gated closed conduits having free surface flow, but result comparisons should not be made if conduit geometries are not similar.
2. The ratio of upstream head-to-gate opening produced a linear relationship with air demand when conduit geometry remained constant.
3. Increased gate roughness (serration) was found to increase water surface roughness and correspondingly the air-demand ratio.
4. Water surface roughness due to turbulence and high water velocity cause higher air demand than water surface roughness due to wave action at low water velocities.

5. Conduit slope did not increase air demand, although it did alter the Froude number for otherwise identical tests.
6. Conduit length significantly affected air demand measured at the air intake, although it was not proportional to length. Thus it can be concluded that a significant amount of air entrainment occurs near the upstream end of the conduit near the downstream side of the gate.
7. This research indicated that there was no noticeable air velocity distribution above the air-water interface for this experiment as suggested by previous researchers.

The following recommendations are made to researchers for further the study of the current research topic:

1. Tests should be conducted at higher flow rates, and higher total upstream energy head and associated Froude numbers to gain a larger range of flow conditions.
2. Multiple models of different scales should be studied to determine if any scale effects exist.
3. Future experimental setups should be built entirely out of clear material to provide flow visualization and provide the ability to observe the air flow pattern above the air-water interface using smoke or other methods.
4. Air flow should be measured at the outlet of the conduit to better understand the differences in air demand for different variables.

REFERENCES

Campbell, F. B., and B. Guyton. 1953. Air demand in gated outlet works. Proceedings of the 5th Congress on the International Association of Hydraulic Research, Minnesota.

Falvey, H. T. 1980. Air-water flow in hydraulic structures. Engineering Monograph 41. U.S. Department of the Interior, Water and Power Resources Service, Denver, Colorado.

Finnemore, E. J., and J. B. Franzini. 2002. Fluid mechanics with engineering applications. McGraw Hill, New York, pp. 158.

Ghetti, A., and G. Di Silvio. 1967. Investigation on the running of deep gated outlet works from reservoirs. Proceedings of the 9th International Congress on Large Dams, Istanbul, Turkey, Vol. 2, Q33 (R48), pp. 837-852.

Kalinske, A. A., and J. W. Robertson. 1943. Closed conduit flow. ASCE Transactions 108: 1435-1447.

Lysne, D. K., and O. Guttormsen. 1971. Air demand in high regulated outlet works. Proceedings of the 14th Congress of the International Association of Hydraulic Research, Vol. 5, Paris, France.

Mifkovic, C. 2007. Success dam outlet works. Unpublished manuscript, United States Army Corps of Engineers, Sacramento, California.

Sharma, H. R. 1976. Air-entrainment in high head gated conduits. ASCE Journal of the Hydraulics Division 102(HY 11): 1629-1646.

Speerli, J. 1999. Air entrainment of free-surface tunnel flow. Proceedings of the 28th IAHR Congress, Graz, Austria, 1999.

Speerli, J., and W. H. Hager. 2000. Air-water flow in bottom outlets. Canadian Journal of Civil Engineering 27: 454-462.

USACE (United States Army Corps of Engineers). 1964. Air demand-regulated outlet works. Hydraulic Design Criteria, Sheet 050-1/2/3, 211-1/2, 255-1.

USACE (United States Army Corps of Engineers). 1980. Hydraulic design of reservoir outlet works. Engineer Manual 1110-2-1602.

APPENDICES

Appendix A: Orifice Meter Calibration

Flow metering for the physical model was accomplished using orifice meters calibrated at the UWRL. Standard methods were used in the calibration of the 6.5-in diameter orifice plate installed in the 8-in supply line and the 9.6-in diameter orifice installed in the 12-in supply line. Figures 10 and 11 show the calibration relationship between the orifice discharge coefficient and Reynolds number for the 8-in orifice and 12-in orifice, respectively.

Discharge coefficients determined for the 8-in orifice calibration had a deviation of 0.39 percent from average with an uncertainty of 0.20 percent. The 12-in orifice discharge coefficients fell within a 0.31 percent deviation from average with an uncertainty of 0.33 percent. Linear equations for discharge coefficient (Cd) and Reynolds number (Re) were fit to the calculated discharge coefficients for each orifice,

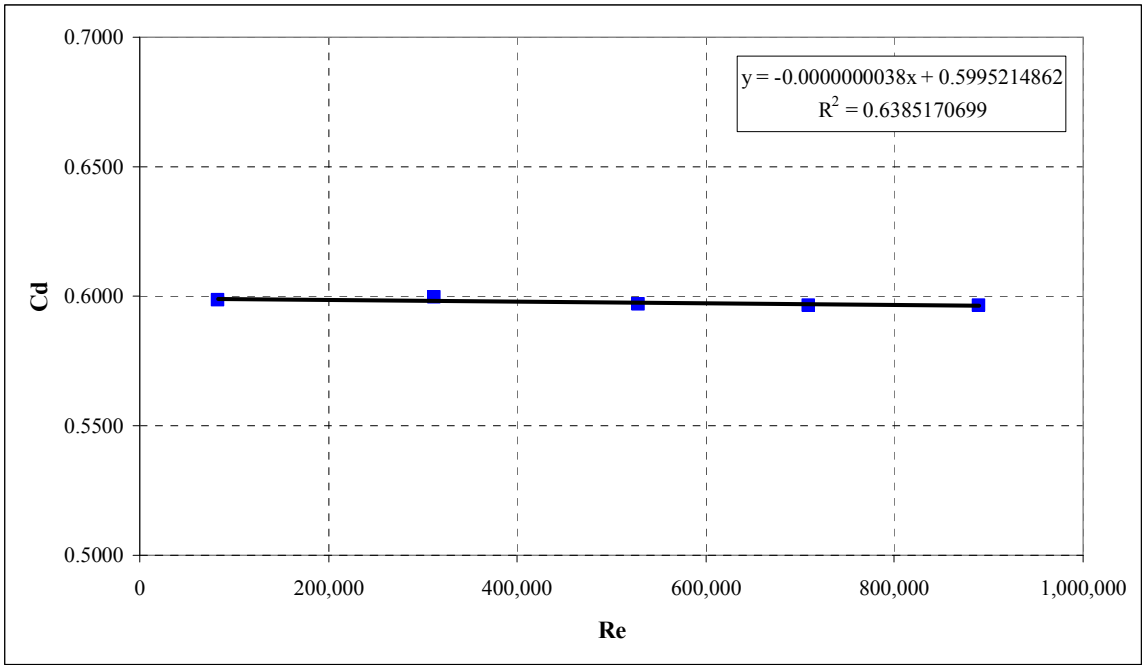

Figure 28. 8-in Orifice Calibration.

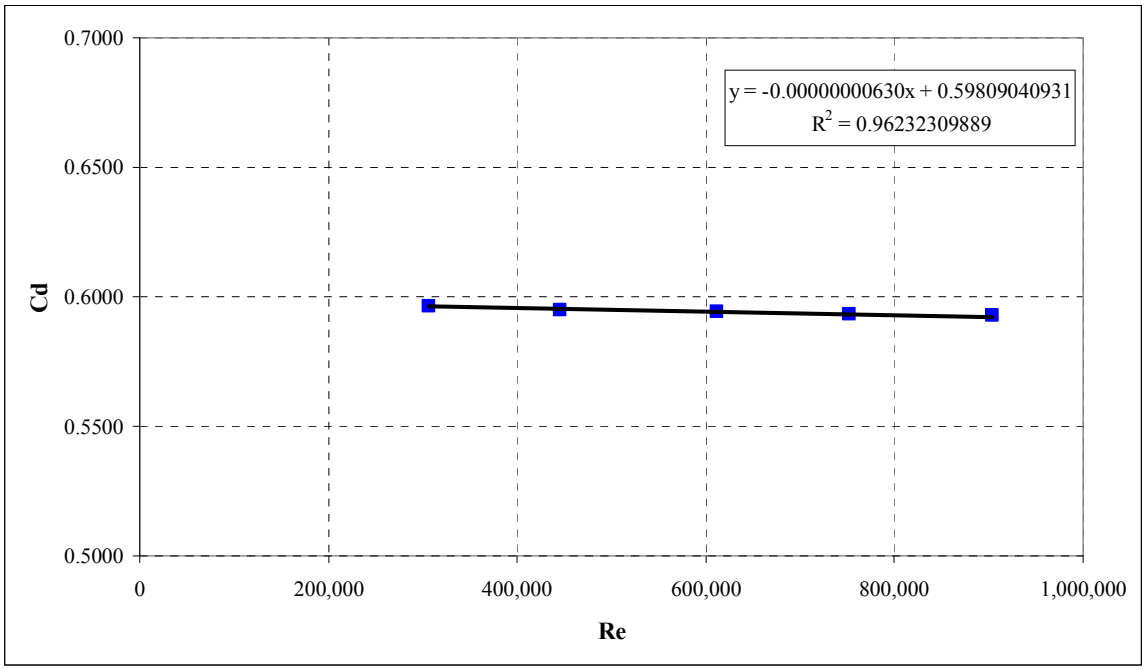

Figure 29. 12-in Orifice Calibration.

their respective R^2 and equation values are shown in. Each orifice was assembled in its respective pipeline before calibration and was then installed directly in the supply line pre-assembled to ensure that each orifice calibration maintained accurate

Appendix B: Air Demand Data

Table 8. Model configuration for each test run

Configuration	Run	Slope	Gate Opening	Gate Depth	Length (ft)	End Cap
1	1A	2.50%	90%	0.8356-ft	48-ft	No
1	1B	2.50%	90%	0.8356-ft	48-ft	No
1	1C	2.50%	90%	0.8356-ft	48-ft	No
2	2A	2.50%	70%	0.6537-ft	48-ft	No
2	2B	2.50%	70%	0.6537-ft	48-ft	No
2	2C	2.50%	70%	0.6537-ft	48-ft	No
3	3B	2.50%	70%	0.6537-ft	48-ft	Yes
4	4A	2.50%	50%	0.4962-ft	48-ft	No
4	4B	2.50%	50%	0.4962-ft	48-ft	No
4	4C	2.50%	50%	0.4962-ft	48-ft	No
5	5A	2.50%	50%	0.4962-ft	48-ft	Yes
5	5B	2.50%	50%	0.4962-ft	48-ft	Yes
6	6A	2.50%	50%	0.4962-ft	29-ft	No
6	6B	2.50%	50%	0.4962-ft	29-ft	No
7	7A	2.50%	50%	0.4962-ft	29-ft	Yes
7	7B	2.50%	50%	0.4962-ft	29-ft	Yes
8	8A	2.50%	50% Rough	0.4962-ft	48-ft	No
8	8B	2.50%	50% Rough	0.4962-ft	48-ft	No
9	9A	2.50%	50% Rough	0.4962-ft	48-ft	Yes
9	9B	2.50%	50% Rough	0.4962-ft	48-ft	Yes
10	10A	2.50%	50% Rough	0.4962-ft	29-ft	No
10	10B	2.50%	50% Rough	0.4962-ft	29-ft	No
11	11A	2.50%	50% Rough	0.4962-ft	29-ft	Yes
11	11B	2.50%	50% Rough	0.4962-ft	29-ft	Yes
12	12A	2.50%	30%	0.3372-ft	48-ft	No
12	12B	2.50%	30%	0.3372-ft	48-ft	No
12	12C	2.50%	30%	0.3372-ft	48-ft	No
13	13B	2.50%	10%	0.1549-ft	48-ft	No
14	14B	2.50%	10%	0.1549-ft	48-ft	Yes
15	15A	0.15%	70%	0.6537-ft	48-ft	No
15	15C	0.15%	70%	0.6537-ft	48-ft	No
15	15B	0.15%	70%	0.6537-ft	48-ft	No
16	16A	0.15%	70%	0.6537-ft	48-ft	Yes
16	16C	0.15%	70%	0.6537-ft	48-ft	Yes
16	16B	0.15%	70%	0.6537-ft	48-ft	Yes
17	17A	0.15%	50%	0.4962-ft	48-ft	No
17	17C	0.15%	50%	0.4962-ft	48-ft	No
17	17B	0.15%	50%	0.4962-ft	48-ft	No
18	18A	0.15%	50%	0.4962-ft	48-ft	Yes
18	18C	0.15%	50%	0.4962-ft	48-ft	Yes
18	18B	0.15%	50%	0.4962-ft	48-ft	Yes
19	19A	0.15%	50%	0.4962-ft	29-ft	No
19	19B	0.15%	50%	0.4962-ft	29-ft	No
20	20A	0.15%	50%	0.4962-ft	29-ft	Yes
20	20B	0.15%	50%	0.4962-ft	29-ft	Yes
21	21A	0.15%	50% Rough	0.4962-ft	48-ft	No
21	21C	0.15%	50% Rough	0.4962-ft	48-ft	No
21	21B	0.15%	50% Rough	0.4962-ft	48-ft	No
22	22A	0.15%	50% Rough	0.4962-ft	48-ft	Yes
22	22C	0.15%	50% Rough	0.4962-ft	48-ft	Yes
22	22B	0.15%	50% Rough	0.4962-ft	48-ft	Yes
23	23A	0.15%	50% Rough	0.4962-ft	29-ft	No
23	23B	0.15%	50% Rough	0.4962-ft	29-ft	No
24	24A	0.15%	50% Rough	0.4962-ft	29-ft	Yes
24	24B	0.15%	50% Rough	0.4962-ft	29-ft	Yes
25	25A	0.15%	30%	0.3372-ft	48-ft	No
25	25C	0.15%	30%	0.3372-ft	48-ft	No
25	25B	0.15%	30%	0.3372-ft	48-ft	No
26	26A	0.15%	30%	0.3372-ft	48-ft	Yes
26	26C	0.15%	30%	0.3372-ft	48-ft	Yes
26	26B	0.15%	30%	0.3372-ft	48-ft	Yes
27	27B	0.15%	10%	0.1549-ft	48-ft	No
28	28B	0.15%	10%	0.1549-ft	48-ft	Yes

Table 9. Air demand and pressure measurements

Configuration	Run	Q_w (cfs)	U/s P (psi)	D/s P	V_a (fpm)	Q_a (cfs)	Q_a/Q_w
1	1A	10.02	0.95	ATM	2050	0.76	0.08
1	1B	8.12	0.65	ATM	1190	0.44	0.05
1	1C	4.82	0.25	ATM	300	0.11	0.02
2	2A	9.00	2.9	ATM	2500	0.93	0.10
2	2B	6.10	1.35	ATM	1051	0.39	0.06
2	2C	3.51	0.25	ATM	360	0.13	0.04
3	3B	6.09	1.15	ATM	1155	0.43	0.07
4	4A	7.47	5.25	ATM	3100	1.15	0.15
4	4B	3.98	1.45	ATM	805	0.30	0.08
4	4C	1.72	0.25	ATM	225	0.08	0.05
5	5A	7.47	5.25	ATM	3020	1.12	0.15
5	5B	3.98	1.45	ATM	840	0.31	0.08
6	6A	7.55	5.2	ATM	2480	0.92	0.12
6	6B	4.26	1.65	ATM	720	0.27	0.06
7	7A	7.55	5.2	ATM	2560	0.95	0.13
7	7B	4.26	1.65	ATM	740	0.27	0.06
8	8A	7.27	4.9	ATM	3585	1.33	0.18
8	8B	3.96	1.4	ATM	933.5	0.35	0.09
9	9A	7.27	4.9	ATM	3625	1.34	0.18
9	9B	3.95	1.4	ATM	932	0.35	0.09
10	10A	7.54	5.2	ATM	3420	1.27	0.17
10	10B	4.26	1.65	ATM	863.5	0.32	0.08
11	11A	7.54	5.2	ATM	3520	1.31	0.17
11	11B	4.26	1.65	ATM	912.5	0.34	0.08
12	12A	5.03	7.75	ATM	2990	1.11	0.22
12	12B	2.98	2.6	ATM	1178.5	0.44	0.15
12	12C	1.39	0.3	ATM	252	0.09	0.07
13	13B	1.04	3.1	ATM	860	0.32	0.31
14	14B	1.04	3.1	ATM	765	0.28	0.27
15	15A	8.98	2.9	ATM	2495	0.93	0.10
15	15C	2.48	0.3	ATM	265	0.10	0.04
15	15B	5.65	1.2	ATM	940	0.35	0.06
16	16A	8.98	2.9	ATM	2510	0.93	0.10
16	16C	2.48	0.3	ATM	237.5	0.09	0.04
16	16B	5.65	1.2	ATM	925	0.34	0.06
17	17A	7.48	5.2	ATM	2875	1.07	0.14
17	17C	1.91	0.3	ATM	220	0.08	0.04
17	17B	4.27	1.65	ATM	856	0.32	0.07
18	18A	7.48	5.2	ATM	2936	1.09	0.15
18	18C	1.91	0.3	ATM	212	0.08	0.04
18	18B	4.27	1.65	ATM	885	0.33	0.08
19	19A	7.51	5.2	ATM	2470	0.92	0.12
19	19B	4.26	1.65	ATM	682.5	0.25	0.06
20	20A	7.51	5.2	ATM	2585	0.96	0.13
20	20B	4.26	1.65	ATM	745	0.28	0.06
21	21A	7.48	5.2	ATM	3560	1.32	0.18
21	21C	1.91	0.3	ATM	238.5	0.09	0.05
21	21B	4.28	1.65	ATM	1045	0.39	0.09
22	22A	7.48	5.2	ATM	3540	1.31	0.18
22	22C	1.91	0.3	ATM	232	0.09	0.05
22	22B	4.28	1.65	ATM	1033	0.38	0.09
23	23A	7.51	5.2	ATM	3465	1.29	0.17
23	23B	4.26	1.65	ATM	823.5	0.31	0.07
24	24A	7.51	5.2	ATM	3475	1.29	0.17
24	24B	4.26	1.65	ATM	854.5	0.32	0.07
25	25A	5.20	8.15	ATM	2940	1.09	0.21
25	25C	1.16	0.3	ATM	188	0.07	0.06
25	25B	3.18	3	ATM	1151	0.43	0.13
26	26A	5.20	8.15	ATM	2912	1.08	0.21
26	26C	1.16	0.3	ATM	190	0.07	0.06
26	26B	3.18	3	ATM	1210	0.45	0.14
27	27B	1.00	3	ATM	731.5	0.27	0.27
28	28B	1.00	3	ATM	666.5	0.25	0.25

Table 10. Water surface depth measurements

Configuration	Run	$Y_{w\ Ave}$ (in)	Y_w 1 (in)	Y_w 2 (in)	Y_w 3 (in)	Y_w 4 (in)	Y_w 5 (in)
1	1A	8.89	8.68	8.62	8.80	9.05	9.30
1	1B	8.70	8.68	8.80	8.68	8.68	8.68
1	1C	7.34	7.74	7.62	7.30	7.05	6.99
2	2A	6.68	6.37	6.55	6.62	6.80	7.05
2	2B	6.02	5.99	5.68	6.05	6.05	6.30
2	2C	5.50	5.49	5.55	5.62	5.30	5.55
3	3B	6.15	6.12	5.93	6.18	6.18	6.37
4	4A	4.99	4.68	4.80	4.93	5.18	5.37
4	4B	4.48	4.12	4.30	4.49	4.68	4.80
4	4C	3.69	3.93	3.93	3.68	3.55	3.37
5	5A	4.99	4.68	4.80	4.93	5.18	5.37
5	5B	4.45	4.05	4.43	4.49	4.62	4.68
6	6A	4.97	4.68	5.05	5.18	NA	NA
6	6B	4.70	4.30	4.80	4.99	NA	NA
7	7A	4.97	4.68	5.05	5.18	NA	NA
7	7B	4.70	4.30	4.80	4.99	NA	NA
8	8A	5.00	5.18	4.68	4.80	5.05	5.30
8	8B	4.50	4.18	4.55	4.43	4.55	4.80
9	9A	5.00	5.18	4.68	4.80	5.05	5.30
9	9B	4.50	4.18	4.55	4.43	4.55	4.80
10	10A	4.85	5.30	4.30	4.93	NA	NA
10	10B	4.68	4.30	4.80	4.93	NA	NA
11	11A	4.85	5.30	4.30	4.93	NA	NA
11	11B	4.68	4.30	4.80	4.93	NA	NA
12	12A	3.65	3.93	3.49	3.24	3.68	3.93
12	12B	3.14	2.80	2.74	3.18	3.49	3.49
12	12C	2.87	3.18	2.55	2.93	2.87	2.80
13	13B	1.62	1.18	0.99	2.18	1.80	1.93
14	14B	1.62	1.18	0.99	2.18	1.80	1.93
15	15A	6.68	6.18	5.68	6.93	7.05	7.55
15	15C	7.25	5.99	6.18	6.93	9.37	7.80
15	15B	6.72	6.30	6.24	6.55	7.05	7.43
16	16A	6.68	6.18	5.68	6.93	7.05	7.55
16	16C	7.25	5.99	6.18	6.93	9.37	7.80
16	16B	6.72	6.30	6.24	6.55	7.05	7.43
17	17A	5.25	4.80	5.05	5.18	5.49	5.74
17	17C	5.00	4.55	4.62	4.93	5.18	5.74
17	17B	4.99	4.30	4.80	4.99	5.30	5.55
18	18A	5.25	4.80	5.05	5.18	5.49	5.74
18	18C	5.00	4.55	4.62	4.93	5.18	5.74
18	18B	4.99	4.30	4.80	4.99	5.30	5.55
19	19A	4.97	4.68	5.05	5.18	NA	NA
19	19B	4.70	4.30	4.80	4.99	NA	NA
20	20A	4.97	4.68	5.05	5.18	NA	NA
20	20B	4.70	4.30	4.80	4.99	NA	NA
21	21A	5.10	5.30	4.30	4.93	5.30	5.68
21	21C	5.07	4.55	4.62	4.87	5.37	5.93
21	21B	4.95	4.30	4.80	4.93	5.18	5.55
22	22A	5.10	5.30	4.30	4.93	5.30	5.68
22	22C	5.07	4.55	4.62	4.87	5.37	5.93
22	22B	4.95	4.30	4.80	4.93	5.18	5.55
23	23A	4.85	5.30	4.30	4.93	NA	NA
23	23B	4.68	4.30	4.80	4.93	NA	NA
24	24A	4.85	5.30	4.30	4.93	NA	NA
24	24B	4.68	4.30	4.80	4.93	NA	NA
25	25A	3.75	3.93	3.43	3.30	3.80	4.30
25	25C	3.59	3.24	3.12	3.68	3.62	4.30
25	25B	3.53	3.12	3.18	3.37	4.12	3.87
26	26A	3.75	3.93	3.43	3.30	3.80	4.30
26	26C	3.59	3.24	3.12	3.68	3.62	4.30
26	26B	3.53	3.12	3.18	3.37	4.12	3.87
27	27B	1.68	1.18	1.18	1.93	2.18	1.93
28	28B	1.68	1.18	1.18	1.93	2.18	1.93

Table 11. Water surface roughness measurements

Configuration	Run	$R_{w\ Ave}$ (in)	R_w 1 (in)	R_w 2 (in)	R_w 3 (in)	R_w 4 (in)	R_w 5 (in)
1	1A	0.29	0.5	0.375	0.375	0.25	0.25
1	1B	0.23	0.375	0.25	0.25	0.25	0.25
1	1C	0.18	0.25	0.25	0.1875	0.25	0.125
2	2A	0.25	0.25	0.375	0.25	0.375	0.25
2	2B	0.25	0.375	0.25	0.25	0.25	0.375
2	2C	0.10	0.125	0.125	0.125	0.125	0.125
3	3B	0.21	0.25	0.25	0.25	0.25	0.25
4	4A	0.33	0.5	0.375	0.375	0.375	0.375
4	4B	0.21	0.25	0.25	0.25	0.25	0.25
4	4C	0.13	0.25	0.125	0.125	0.125	0.125
5	5A	0.33	0.5	0.375	0.375	0.375	0.375
5	5B	0.23	0.25	0.25	0.375	0.25	0.25
6	6A	0.58	0.75	0.5	0.5	NA	NA
6	6B	0.25	0.25	0.25	0.25	NA	NA
7	7A	0.58	0.75	0.5	0.5	NA	NA
7	7B	0.25	0.25	0.25	0.25	NA	NA
8	8A	0.88	1.25	1.25	1	0.875	0.875
8	8B	0.50	0.625	0.625	0.625	0.5	0.625
9	9A	0.88	1.25	1.25	1	0.875	0.875
9	9B	0.50	0.625	0.625	0.625	0.5	0.625
10	10A	1.58	1.5	2	1.25	NA	NA
10	10B	0.58	0.75	0.5	0.5	NA	NA
11	11A	1.58	1.5	2	1.25	NA	NA
11	11B	0.58	0.75	0.5	0.5	NA	NA
12	12A	0.27	0.375	0.375	0.375	0.25	0.25
12	12B	0.21	0.25	0.25	0.25	0.25	0.25
12	12C	0.10	0.125	0.125	0.125	0.125	0.125
13	13B	0.21	0.25	0.25	0.25	0.25	0.25
14	14B	0.21	0.25	0.25	0.25	0.25	0.25
15	15A	0.44	0.75	0.5	0.5	0.5	0.375
15	15C	0.08	0.125	0.125	0.125	0.0625	0.0625
15	15B	0.21	0.25	0.25	0.25	0.25	0.25
16	16A	0.44	0.75	0.5	0.5	0.5	0.375
16	16C	0.08	0.125	0.125	0.125	0.0625	0.0625
16	16B	0.21	0.25	0.25	0.25	0.25	0.25
17	17A	0.33	0.5	0.375	0.375	0.375	0.375
17	17C	0.10	0.125	0.125	0.125	0.125	0.125
17	17B	0.21	0.25	0.25	0.25	0.25	0.25
18	18A	0.33	0.5	0.375	0.375	0.375	0.375
18	18C	0.10	0.125	0.125	0.125	0.125	0.125
18	18B	0.21	0.25	0.25	0.25	0.25	0.25
19	19A	0.58	0.75	0.5	0.5	NA	NA
19	19B	0.25	0.25	0.25	0.25	NA	NA
20	20A	0.58	0.75	0.5	0.5	NA	NA
20	20B	0.25	0.25	0.25	0.25	NA	NA
21	21A	0.92	1.25	1.25	1.25	0.875	0.875
21	21C	0.29	0.375	0.375	0.375	0.25	0.375
21	21B	0.48	0.75	0.625	0.5	0.5	0.5
22	22A	0.92	1.25	1.25	1.25	0.875	0.875
22	22C	0.29	0.375	0.375	0.375	0.25	0.375
22	22B	0.48	0.75	0.625	0.5	0.5	0.5
23	23A	1.58	1.5	2	1.25	NA	NA
23	23B	0.58	0.75	0.5	0.5	NA	NA
24	24A	1.58	1.5	2	1.25	NA	NA
24	24B	0.58	0.75	0.5	0.5	NA	NA
25	25A	0.52	0.75	0.5	0.5	0.75	0.625
25	25C	0.10	0.125	0.125	0.125	0.125	0.125
25	25B	0.25	0.375	0.375	0.25	0.25	0.25
26	26A	0.52	0.75	0.5	0.5	0.75	0.625
26	26C	0.10	0.125	0.125	0.125	0.125	0.125
26	26B	0.25	0.375	0.375	0.25	0.25	0.25
27	27B	0.33	0.5	0.5	0.25	0.25	0.5
28	28B	0.33	0.5	0.5	0.25	0.25	0.5

Appendix C: Air Profile Data

Air profile data was obtained by using the air velocity probe as discussed in the data measurement section in Chapter 3. Occasional data was obtained for the air velocity at the exit of the conduit and is labeled as Station 6. As discussed previously it was hard to determine a direction for each measurement. Velocity direction is indicated by the sign of the velocity measurement at each point, a positive velocity measurement means that the air was traveling downstream the conduit, while a negative velocity measurement means that the air was traveling upstream the conduit. Velocity directions were only verified for Station 1 and Station 6 data using smoke visualization. All other data obtained in the non-clear PVC pipe sections has been given a direction of positive or downstream, this has not been verified and might not be correct. The following tables outline all velocity profile measurements for the 2.5 percent slope.

Table 12. Air profile data for run 1A

Station #	x (ft)	Yw (in)	Rw (in)	Vw (fps)	Ya 1 (in)	Va 1 (fps)	Ya 2 (in)	Va 2(fps)	Ya 3 (in)	Va 3 (fps)
1	5	8.68	0.50	16.62	11.65	NA	11.46	NA	11.27	NA
2	15	8.62	0.38	16.75	11.65	2.17	11.37	NA	11.09	NA
3	25	8.80	0.38	16.37	11.65	1.67	11.46	NA	11.27	NA
4	35	9.05	0.25	15.91	11.65	2.00	11.52	NA	11.40	NA
5	45	9.30	0.25	15.48	11.65	1.42	11.65	NA	11.65	NA

Table 13. Air profile data for run 1B

Station #	x (ft)	Yw (in)	Rw (in)	Vw (fps)	Ya 1 (in)	Va 1 (fps)	Ya 2 (in)	Va 2(fps)	Ya 3 (in)	Va 3 (fps)
1	5	8.68	0.38	13.47	11.65	-2.47	11.40	2.17	11.15	2.33
2	15	8.80	0.25	13.27	11.65	2.25	11.40	1.75	11.15	1.92
3	25	8.68	0.25	13.47	11.65	1.33	11.34	1.33	11.02	1.42
4	35	8.68	0.25	13.47	11.65	1.32	11.34	1.08	11.02	1.37
5	45	8.68	0.25	13.47	11.65	1.33	11.34	1.08	11.02	1.25

Table 14. Air profile data for run 1C

Station #	x (ft)	Yw (in)	Rw (in)	Vw (fps)	Ya 1 (in)	Va 1 (fps)	Ya 2 (in)	Va 2(fps)	Ya 3 (in)	Va 3 (fps)
1	5	7.74	0.25	9.06	11.65	-1.03	10.87	1.22	10.09	1.28
2	15	7.62	0.25	9.23	11.65	1.28	10.81	1.32	9.96	0.83
3	25	7.30	0.19	9.70	11.65	1.20	10.62	1.65	9.59	1.50
4	35	7.05	0.25	10.11	11.65	1.13	10.52	1.70	9.40	1.70
5	45	6.99	0.13	10.22	11.65	1.28	10.43	1.78	9.21	1.58

Table 15. Air profile data for run 2A

Station #	x (ft)	Yw (in)	Rw (in)	Vw (fps)	Ya 1 (in)	Va 1 (fps)	Ya 2 (in)	Va 2(fps)	Ya 3 (in)	Va 3 (fps)
1	5	6.37	0.25	21.42	11.65	-12.33	10.18	NA	8.71	NA
2	15	6.55	0.38	20.66	11.65	7.00	10.34	NA	9.02	NA
3	25	6.62	0.25	20.42	11.65	4.58	10.31	NA	8.96	NA
4	35	6.80	0.38	19.74	11.65	3.33	10.46	NA	9.27	NA
5	45	7.05	0.25	18.89	11.65	2.67	10.52	NA	9.40	NA

Table 16. Air profile data for run 2B

Station #	x (ft)	Yw (in)	Rw (in)	Vw (fps)	Ya 1 (in)	Va 1 (fps)	Ya 2 (in)	Va 2(fps)	Ya 3 (in)	Va 3 (fps)
1	5	5.99	0.38	15.66	11.65	-4.32	10.21	2.75	8.77	9.75
2	15	5.68	0.25	16.77	11.65	1.88	10.21	1.53	8.77	2.92
3	25	6.05	0.25	15.45	11.65	1.24	10.21	1.34	8.77	2.04
4	35	6.05	0.25	15.45	11.65	1.15	10.21	1.10	8.77	1.54
5	45	6.30	0.38	14.69	11.65	1.39	10.21	1.01	8.77	1.71
6	48	6.30	0.38	14.69	11.65	-0.78	10.21	0.82	8.77	0.80

Table 17. Air profile data for run 2C

Station #	x (ft)	Yw (in)	Rw (in)	Vw (fps)	Ya 1 (in)	Va 1 (fps)	Ya 2 (in)	Va 2(fps)	Ya 3 (in)	Va 3 (fps)
1	5	6.12	0.25	15.24	11.65	-4.95	10.21	3.25	8.77	2.32
2	15	5.93	0.25	15.85	11.65	1.99	10.21	1.78	8.77	2.77
3	25	6.18	0.25	15.04	11.65	1.29	10.21	1.26	8.77	1.79
4	35	6.18	0.25	15.04	11.65	1.33	10.21	1.04	8.77	1.41
5	45	6.37	0.25	14.49	11.65	1.43	10.21	0.96	8.77	1.52

Table 18. Air profile data for run 3B

Station #	x (ft)	Yw (in)	Rw (in)	Vw (fps)	Ya 1 (in)	Va 1 (fps)	Ya 2 (in)	Va 2(fps)	Ya 3 (in)	Va 3 (fps)
1	5	5.49	0.13	10.08	11.65	-1.83	9.74	1.58	7.84	1.28
2	15	5.55	0.13	9.93	11.65	1.63	9.74	1.75	7.84	1.27
3	25	5.62	0.13	9.79	11.65	1.31	9.74	1.45	7.84	1.53
4	35	5.30	0.13	10.55	11.65	1.32	9.74	1.44	7.84	1.67
5	45	5.55	0.13	9.93	11.65	1.43	9.74	1.47	7.84	1.27

Table 19. Air profile data for run 4A

Station #	x (ft)	Yw (in)	Rw (in)	Vw (fps)	Ya 1 (in)	Va 1 (fps)	Ya 2 (in)	Va 2(fps)	Ya 3 (in)	Va 3 (fps)
1	5	4.68	0.25	26.53	11.65	NA	9.93	NA	8.21	NA
2	15	4.80	0.25	25.61	11.65	10.83	9.93	8.17	8.21	NA
3	25	4.93	0.25	24.75	11.65	6.25	9.93	5.79	8.21	NA
4	35	5.18	0.25	23.18	11.65	5.83	9.93	5.12	8.21	NA
5	45	5.37	0.25	22.13	11.65	5.08	9.93	3.43	8.21	NA
6	48	5.37	0.25	22.13	11.65	-1.50	9.93	0.97	8.21	NA

Table 20. Air profile data for run 4B

Station #	x (ft)	Yw (in)	Rw (in)	Vw (fps)	Ya 1 (in)	Va 1 (fps)	Ya 2 (in)	Va 2(fps)	Ya 3 (in)	Va 3 (fps)
1	5	4.68	0.25	26.53	11.65	NA	9.93	NA	8.21	NA
2	15	4.80	0.25	25.61	11.65	11.08	9.90	10.83	8.21	NA
3	25	4.93	0.25	24.75	11.65	6.42	9.93	9.17	8.21	NA
4	35	5.18	0.25	23.18	11.65	6.08	9.93	4.25	8.21	NA
5	45	5.37	0.25	22.13	11.65	5.85	9.93	4.35	8.21	NA

Table 21. Air profile data for run 4C

Station #	x (ft)	Yw (in)	Rw (in)	Vw (fps)	Ya 1 (in)	Va 1 (fps)	Ya 2 (in)	Va 2(fps)	Ya 3 (in)	Va 3 (fps)
1	5	4.12	0.25	16.78	11.65	-1.83	9.40	2.28	7.15	2.58
2	15	4.30	0.25	15.80	11.65	1.42	9.40	2.20	7.15	2.50
3	25	4.49	0.25	14.91	11.65	1.33	9.40	0.93	7.15	1.77
4	35	4.68	0.25	14.11	11.65	1.10	9.40	0.94	7.15	1.60
5	45	4.80	0.25	13.63	11.65	1.04	9.40	0.95	7.15	1.64
6	48	4.80	0.25	13.63	11.65	-0.67	9.40	0.63	7.15	0.77

Table 22. Air profile data for run 5A

Station #	x (ft)	Yw (in)	Rw (in)	Vw (fps)	Ya 1 (in)	Va 1 (fps)	Ya 2 (in)	Va 2(fps)	Ya 3 (in)	Va 3 (fps)
1	5	4.05	0.25	17.14	11.65	-2.01	9.40	1.71	7.15	2.16
2	15	4.43	0.25	15.20	11.65	2.00	9.40	2.16	7.15	2.34
3	25	4.49	0.38	14.91	11.65	0.98	9.40	0.98	7.15	1.64
4	35	4.62	0.25	14.37	11.65	0.98	9.40	1.03	7.15	1.43
5	45	4.68	0.25	14.11	11.65	0.89	9.40	1.03	7.15	1.33

Table 23. Air profile data for run 5B

Station #	x (ft)	Yw (in)	Rw (in)	Vw (fps)	Ya 1 (in)	Va 1 (fps)	Ya 2 (in)	Va 2(fps)	Ya 3 (in)	Va 3 (fps)
1	5	3.93	0.25	7.71	11.65	-0.79	8.96	0.96	6.27	0.29
2	15	3.93	0.13	7.71	11.65	1.14	8.96	1.37	6.27	0.73
3	25	3.68	0.13	8.44	11.65	1.09	8.96	1.25	6.27	0.61
4	35	3.55	0.13	8.86	11.65	1.16	8.96	1.29	6.27	0.97
5	45	3.37	0.13	9.55	11.65	1.26	8.96	1.26	6.27	0.60
6	48	3.37	0.13	9.55	11.65	-0.37	8.96	0.22	6.27	0.23

Table 24. Air profile data for run 6A

Station #	x (ft)	Yw (in)	Rw (in)	Vw (fps)	Ya 1 (in)	Va 1 (fps)	Ya 2 (in)	Va 2(fps)	Ya 3 (in)	Va 3 (fps)
1	5	4.62	0.50	27.25	11.65	NA	9.93	NA	8.21	NA
2	15	4.68	0.50	26.76	11.65	10.08	9.93	NA	8.21	NA
3	25	4.87	0.50	25.39	11.65	5.77	9.93	NA	8.21	NA
4	35	5.18	0.50	23.38	11.65	5.39	9.93	NA	8.21	NA
5	45	5.30	0.50	22.66	11.65	4.50	9.93	NA	8.21	NA
6	48	5.30	0.50	22.66	11.65	-1.58	9.93	NA	8.21	NA

Table 25. Air profile data for run 6B

Station #	x (ft)	Yw (in)	Rw (in)	Vw (fps)	Ya 1 (in)	Va 1 (fps)	Ya 2 (in)	Va 2(fps)	Ya 3 (in)	Va 3 (fps)
1	5	4.55	0.50	27.75	11.65	NA	9.93	NA	8.21	NA
2	15	4.74	0.50	26.29	11.65	6.29	9.93	NA	8.21	NA
3	25	4.93	0.50	24.96	11.65	5.08	9.93	NA	8.21	NA
4	35	5.05	1.00	24.15	11.65	4.83	9.93	NA	8.21	NA
5	45	5.37	0.63	22.32	11.65	3.75	9.93	NA	8.21	NA

Table 26. Air profile data for run 7A

Station #	x (ft)	Yw (in)	Rw (in)	Vw (fps)	Ya 1 (in)	Va 1 (fps)	Ya 2 (in)	Va 2(fps)	Ya 3 (in)	Va 3 (fps)
1	5	4.18	0.25	16.40	11.65	-2.83	9.40	2.59	7.15	2.71
2	15	4.43	0.38	15.16	11.65	2.09	9.40	1.88	7.15	2.54
3	25	4.55	0.25	14.60	11.65	1.07	9.40	1.07	7.15	1.80
4	35	4.62	0.38	14.34	11.65	1.08	9.40	0.91	7.15	1.43
5	45	4.80	0.25	13.59	11.65	1.24	9.40	0.85	7.15	1.44
6	48	4.80	0.25	13.59	11.65	-0.42	9.40	0.26	7.15	0.34

Table 27. Air profile data for run 7B

Station #	x (ft)	Yw (in)	Rw (in)	Vw (fps)	Ya 1 (in)	Va 1 (fps)	Ya 2 (in)	Va 2(fps)	Ya 3 (in)	Va 3 (fps)
1	5	4.30	0.25	15.76	11.27	-2.77	9.40	1.78	7.15	1.83
2	15	4.43	0.38	15.16	11.27	1.98	9.40	1.42	7.15	1.77
3	25	4.55	0.25	14.60	11.27	0.93	9.40	0.66	7.15	1.23
4	35	4.62	0.25	14.34	11.27	1.05	9.40	0.78	7.15	1.04
5	45	4.74	0.38	13.83	11.27	1.06	9.40	0.45	7.15	0.63

Table 28. Air profile data for run 8A

Station #	x (ft)	Yw (in)	Rw (in)	Vw (fps)	Ya 1 (in)	Va 1 (fps)	Ya 2 (in)	Va 2(fps)	Ya 3 (in)	Va 3 (fps)
1	5	3.93	0.25	7.68	11.65	-0.32	8.96	0.88	6.27	0.34
2	15	3.80	0.25	8.03	11.65	0.83	8.96	1.31	6.27	0.45
3	25	3.74	0.25	8.21	11.65	0.69	8.96	1.24	6.27	0.48
4	35	3.55	0.25	8.82	11.65	0.74	8.96	1.42	6.27	0.92
5	45	3.43	0.25	9.27	11.65	0.92	8.96	1.37	6.27	0.29
6	48	3.43	0.25	9.27	11.65	-0.21	8.96	0.29	6.27	0.00

Table 29. Air profile data for run 8B

Station #	x (ft)	Yw (in)	Rw (in)	Vw (fps)	Ya 1 (in)	Va 1 (fps)	Ya 2 (in)	Va 2(fps)	Ya 3 (in)	Va 3 (fps)
1	5	5.18	1.25	22.55	11.65	NA	8.96	NA	6.27	NA
2	15	4.68	1.00	25.80	11.65	8.05	8.96	NA	6.27	NA
3	25	4.80	1.00	24.91	11.65	3.13	8.96	NA	6.27	NA
4	35	5.05	0.88	23.28	11.65	2.38	8.96	NA	6.27	NA
5	45	5.30	0.88	21.85	11.65	1.83	8.96	NA	6.27	NA
6	48	5.30	0.88	21.85	11.65	-0.78	8.96	NA	6.27	NA

Table 30. Air profile data for run 9A

Station #	x (ft)	Yw (in)	Rw (in)	Vw (fps)	Ya 1 (in)	Va 1 (fps)	Ya 2 (in)	Va 2(fps)	Ya 3 (in)	Va 3 (fps)
1	5	5.18	1.25	22.55	11.65	NA	8.96	NA	6.27	NA
2	15	4.68	1.00	25.80	11.65	10.38	8.96	NA	6.27	NA
3	25	4.80	1.00	24.91	11.65	4.53	8.96	NA	6.27	NA
4	35	5.05	0.88	23.28	11.65	3.86	8.96	NA	6.27	NA
5	45	5.30	0.88	21.85	11.65	3.67	8.96	NA	6.27	NA

Table 31. Air profile data for run 9B

Station #	x (ft)	Yw (in)	Rw (in)	Vw (fps)	Ya 1 (in)	Va 1 (fps)	Ya 2 (in)	Va 2(fps)	Ya 3 (in)	Va 3 (fps)
1	5	4.18	0.63	16.36	11.65	-3.08	9.59	2.07	7.52	3.67
2	15	4.55	0.63	14.57	11.65	2.01	9.59	1.42	7.52	1.63
3	25	4.43	0.63	15.12	11.65	1.03	9.59	0.34	7.52	1.16
4	35	4.55	0.50	14.57	11.65	1.01	9.59	0.35	7.52	1.00
5	45	4.80	0.63	13.56	11.65	0.78	9.59	0.32	7.52	0.81
6	48	4.80	0.63	13.56	11.65	-0.36	9.59	0.00	7.52	0.00

Table 32. Air profile data for run 10A

Station #	x (ft)	Yw (in)	Rw (in)	Vw (fps)	Ya 1 (in)	Va 1 (fps)	Ya 2 (in)	Va 2(fps)	Ya 3 (in)	Va 3 (fps)
1	5	4.18	0.63	16.32	11.65	-3.49	9.59	2.46	7.52	3.50
2	15	4.55	0.63	14.53	11.65	2.13	9.59	1.58	7.52	1.88
3	25	4.43	0.63	15.09	11.65	1.13	9.59	0.84	7.52	1.22
4	35	4.55	0.50	14.53	11.65	1.17	9.59	0.78	7.52	1.03
5	45	4.80	0.63	13.53	11.65	0.93	9.59	0.39	7.52	0.92

Table 33. Air profile data for run 10B

Station #	x (ft)	Yw (in)	Rw (in)	Vw (fps)	Ya 1 (in)	Va 1 (fps)	Ya 2 (in)	Va 2(fps)	Ya 3 (in)	Va 3 (fps)
1	5	3.93	0.38	22.64	11.65	NA	9.02	NA	6.40	NA
2	15	3.49	0.38	26.65	11.65	12.99	9.02	NA	6.40	NA
3	25	3.24	0.38	29.56	11.65	5.00	9.02	NA	6.40	NA
4	35	3.68	0.25	24.79	11.65	4.17	9.02	NA	6.40	NA
5	45	3.93	0.25	22.64	11.65	3.42	9.02	NA	6.40	NA
6	48	3.93	0.25	22.64	11.65	-1.62	9.02	NA	6.40	NA

Table 34. Air profile data for run 11A

Station #	x (ft)	Yw (in)	Rw (in)	Vw (fps)	Ya 1 (in)	Va 1 (fps)	Ya 2 (in)	Va 2(fps)	Ya 3 (in)	Va 3 (fps)
1	5	2.80	0.25	21.46	11.65	-2.28	5.84	2.50	8.74	1.88
2	15	2.74	0.25	22.16	11.65	2.59	5.84	3.14	8.74	2.33
3	25	3.18	0.25	17.98	11.65	1.70	5.84	1.93	8.74	1.44
4	35	3.49	0.25	15.77	11.65	1.64	5.84	1.63	8.74	1.42
5	45	3.49	0.25	15.77	11.65	1.20	5.84	1.37	8.74	0.30

Table 35. Air profile data for run 11B

Station #	x (ft)	Yw (in)	Rw (in)	Vw (fps)	Ya 1 (in)	Va 1 (fps)	Ya 2 (in)	Va 2(fps)	Ya 3 (in)	Va 3 (fps)
1	5	3.18	0.13	8.39	11.65	-0.81	5.40	0.38	8.52	1.69
2	15	2.55	0.13	11.43	11.65	1.03	5.40	1.13	8.52	1.53
3	25	2.93	0.13	9.41	11.65	1.17	5.15	1.47	8.37	1.48
4	35	2.87	0.13	9.70	11.65	1.16	5.09	1.09	8.37	1.45
5	45	2.80	0.13	10.01	11.65	1.34	5.40	0.41	8.52	1.34
6	48	2.80	0.13	10.01	11.65	-0.66	8.52	0.29	5.40	0.33

Table 36. Air profile data for run 12A

Station #	x (ft)	Yw (in)	Rw (in)	Vw (fps)	Ya 1 (in)	Va 1 (fps)	Ya 2 (in)	Va 2(fps)	Ya 3 (in)	Va 3 (fps)
1	5	NA	NA	NA	NA	NA	NA	NA	NA	NA
2	15	1.30	1.25	41.46	11.65	11.83	4.65	NA	8.15	NA
3	25	1.93	0.38	23.45	11.65	7.67	4.65	NA	8.15	NA
4	35	1.99	0.38	22.39	11.65	3.64	4.65	NA	8.15	NA
5	45	2.05	0.25	21.42	11.65	2.00	4.65	NA	8.15	NA
6	48	2.05	0.25	21.42	11.65	-0.53	8.15	NA	4.65	NA

Table 37. Air profile data for run 12B

Station #	x (ft)	Yw (in)	Rw (in)	Vw (fps)	Ya 1 (in)	Va 1 (fps)	Ya 2 (in)	Va 2(fps)	Ya 3 (in)	Va 3 (fps)
1	5	1.18	0.25	26.30	11.65	-3.46	4.52	NA	8.09	2.53
2	15	0.99	0.25	33.94	11.65	1.57	4.52	2.69	8.09	2.39
3	25	2.18	0.25	10.76	11.65	1.29	4.52	1.42	8.09	1.21
4	35	1.80	0.25	14.14	11.65	0.64	4.52	0.94	8.09	0.50
5	45	1.93	0.25	12.83	11.65	0.88	4.52	0.73	8.09	0.37
6	48	1.93	0.25	12.83	11.65	0.00	8.09	0.00	4.52	0.00

Table 38. Air profile data for run 12C

Station #	x (ft)	Yw (in)	Rw (in)	Vw (fps)	Ya 1 (in)	Va 1 (fps)	Ya 2 (in)	Va 2(fps)	Ya 3 (in)	Va 3 (fps)
1	5	1.18	0.25	26.30	11.65	-1.91	4.52	NA	8.09	2.63
2	15	0.99	0.25	33.94	11.65	0.93	4.52	2.89	8.09	2.43
3	25	2.18	0.25	10.76	11.65	0.98	4.52	1.54	8.09	1.20
4	35	1.80	0.25	14.14	11.65	0.41	4.52	1.07	8.09	0.42
5	45	1.93	0.25	12.83	11.65	0.35	4.52	0.88	8.09	0.33